Thruster Development Set-up for the Helicon Plasma Hydrazine Combined Micro Research Project (HPH.com)

IEPC-2011-241

Presented at the 32nd International Electric Propulsion Conference,
Wiesbaden • Germany
September 11 – 15, 2011

D. Pavarin[1], F. Ferri[2], M. Manente[3], A. Lucca Fabris[4], F. Trezzolani[5], M. Faenza[6] and L. Tasinato[7]
Center of Studies and Activities for Space (CISAS) "G.Colombo", University of Padova, Padova, Italy

O. Tudisco[8], R.Deangelis[9]
Agenzia Nazionale per le Nuove Tecnologie l'Energia e lo Sviluppo Economico Sostenibile (ENEA), Frascati, Italy

A. Loyan[10], Y. Protsan[11], A. Tsaglov[12]
National Aerospace University 'Kharkiv Aviation Institute' (KhAI), Kharkiv, Ukraine

A. Selmo[13]
Studio Progettazione e Realizzazione di Apparati Elettronici di Selmo Antonio (RESIA), Albaredo d'Adige, Italy

K. Katsonis [14], Ch. Berenguer [15]
DEDALOS EPE, Thessaloniki, Greece

D. Packan [16], J. Jarrige, C. Blanchard, P.Q. Elias, J. Bonnet
ONERA, Palaiseau, France

Abstract: This paper describes the experimental tests done to support the development of an helicon plasma thruster for small satellites. The thruster class is 50 W 1mN. This work is done within the research project Helicon Plasma Hydrazine Combined Micro (HPH.com) in the frame of the 7th Framework Programme of the EU by an European consortium. Experimental tests are foreseen to validate codes, to support thruster design and to verify thruster performances. Three different test bed have been set-up and operated, two laboratory model and an engineering model have been currently built, a final qualification model is under design. Tests have been conducted at CISAS, KhAI, and ONERA. The following paper present the experimental layout and the test conducted in each laboratory.

[1] Researcher, Department of Mechanical Engineering, Center of Studies and Activities for Space (CISAS), University of Padua, daniele.pavarin@unipd.it
[2] Program manager, Center of Studies and Activities for Space (CISAS), University of Padua, francesca.ferri@unipd.it
[3] Senior Engineer, Center of Studies and Activities for Space (CISAS), University of Padua, marco.manente@unipd.it
[4] Ph.D Student, Center of Studies and Activities for Space (CISAS), University of Padua, andrea.luccafabris@studenti.unipd.it
[5] Junior Engineer, Center of Studies and Activities for Space (CISAS), University of Padua, f.trezzolani@hit09.com
[6] Ph.D Student, Center of Studies and Activities for Space (CISAS), University of Padua, martina.faenza@studenti.unipd.it
[7] Technician, Department of Mechanical Engineering, Center of Studies and Activities for Space (CISAS), University of Padua, luca.tasinato@unipd.it
[8] Researcher, ENEA, onofrio.tudisco@enea.it
[9] Researcher, ENEA, riccardo.deangelis@enea.it
[10] Chief of department, STC SPE KhAI, A.Loyan@Khai.edu
[11] Senior scientist, STC SPE KhAI, yul_pro@ukr.net
[12] Scientist, STC SPE KhAI, A.Tsaglov@ukr.net
[13] Senior Electronic Engineer, RESIA, selmo.ing@tin.it
[14] Director, DEDALOS EPE, katsonis@dedalos.eu
[15] Project Manager, DEDALOS EPE, berenguer@dedalos.eu
[16] Researcher, Physics and Instrumentation Department (DMPH), Onera, denis.packan@onera.fr

I.

Nomenclature

E = spectral emission
C-R = Collisional Radiative
LTE = Local Thermodynamic Equilibrium
n_e = electron density
PIC = Particle in Cell
T_e = electronic temperature
e = electron charge
m_e = electron mass
c = light speed
ε_o = vacuum dielectric constant
RPA = Retarding Potential Analyzer
IEDF = Ion Energy Distribution Function
RF = Radio Frequency
PMEA = Permanent Magnet Electro-Analogous
EM = Engineering Model
SPT = Stationary Plasma Thruster

II. Introduction

THE objective of the HPH.com research program (Helicon Plasma Hydrazine combined micro) is to design, optimize and develop a space plasma thruster based on helicon-radio-frequency technology and its application to a mini-satellite for attitude and position control (Figure 1). Moreover, a detailed feasibility study is also ongoing to evaluate the possibility of using the plasma thruster to heat and or decompose a secondary propellant, in order to develop a two mode thruster, characterized by an high-efficiency low-thrust plasma-thruster mode and a low-efficiency high-trust secondary-propellant plasma-enhanced mode.

Target of this research program are applications in the range of 50-100 W power. Expected thruster performance are: 1.5 mN of thrust and I_{sp} > 1200 s. HPH.com develops through the following steps:

a) Deep numerical-theoretical investigation through dedicated plasma-simulation tools;

b) Extensive experimental campaign to validate codes, to investigate the physics phenomena involved and to prove thruster performance;

c) The development of a full-scale thruster-prototype to be mounted on board of a mini-satellite to demonstrate technology feasibility;

d) The study of all the critical issues related to the application to a mini-satellite;

e) The design and manufacturing of the mini-satellite mock up including all critical components;

f) Analysis of scaling law to lower and higher power;

As a final results of the project, a detailed analysis will be conducted in order to evaluate the possible application of the thruster in space missions requiring low-thrust accurate-attitude and position control. The project is started December 2008 and is currently ongoing. In this paper is presented an overview of the experimental activities done and ongoing.

III. Review of existing experimental set-up

Several helicon experiments have been developed in the past years aiming at developing efficient plasma source for industrial applications and space propulsion. The experimental layout can be classified in two main classes: (i) helicon source mounted externally with respect to the main vacuum chamber[1], and (ii) helicon source mounted internally the main vacuum chamber[2-6].

Magnetic field is generated both with coils [1-4 6-9] and permanent magnets [5,10,13]. Magnetic field strength varies form low magnetic field[2] (lower than 100 Gauss) medium[2,3,4,7,8,11,18] (between 100-1000 G) and high[1,5,6,10,14,15] (>1000 G). Enhancement of plasma density using non-uniform magnetic field has been identified by Braginky[7], Shamrai[10], Yoshitaka[9]. Increasing on magnetic field strength has been achieved Shinohara[19] using a suitable magnetic circuit placed outside the source.

The antenna set-up varies through different well know helicon antenna configurations however the most common are helical [1,2,3,6,9] Nagoya III [3-5,6], Boswell 7[,8,18] bifilar antenna was used by Miljak[4], Gillard [6] tested both helical, Nagoya III and modified Nagoya a single and a 4-loop spiral antennae.

The antenna is most of the time fed by a L-matching network operating at 13.56 MHz. Operations in the range 20-30 MHz has been studied by Miljak[4], Toki [18],Chen [13], 10-100 MHz range was studied by Eom[5] in a remarkable low power regime (20-100 W), Toki[8,18].

Standard diagnostic of plasma sources is normally based on compensated Langmuir probes set-up to scan plasmas

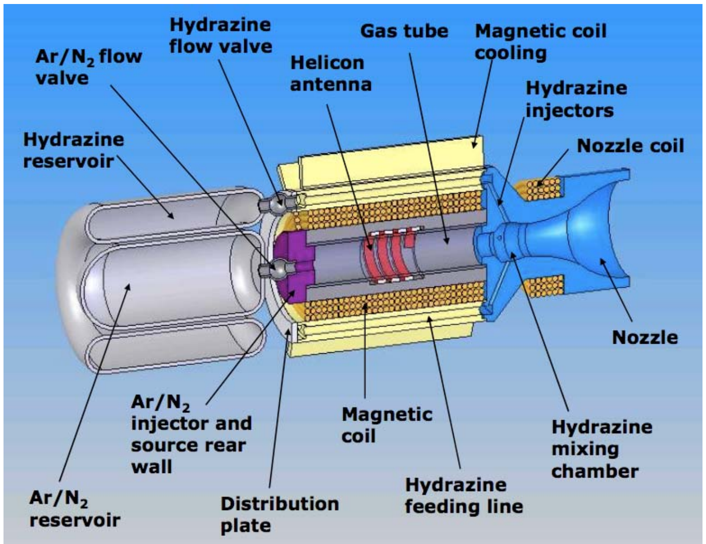

Figure 1. Schematics of the HPH.com helicon thruster.

radially or axially, spectrometer[1], CCD cameras[3], and microwave interferometers[9]. Magnetic probe has been also applied to analyze the helicon field [4,7,16]. The plasma beam is studied using moveable Mach probes[1,14], with RPAs [1,2,7,10,11] and LIF[15].

In Europe , beside the HPH.com study funded by the EC, an helicon thruster prototype is also under development at University of Surrey-EADS Astrium[20].

IV. Model philosophy

Experimental activities are a fundamental step in HPH.com research program. The experimental test bed is under development aiming at:

(i) Code validation: several tests are planned in order to validate the codes under development.

(ii) Thruster analysis and optimization

(iii) Thruster performance characterization

The experimental activities is developing in three laboratories in order to compress the development-time. Laboratory models have been developed and deeply tested at CISAS and KhAi in parallel on different thruster set-up. Based on the outcome of experiment at KkAI an Engineering model (EM) has been also developed and is currently under testing at ONERA. The Engineering model include the all thruster development done at KhAI and is equipped with a standard three loops helicon antenna. The purpose of the EM is to verify the technology applied in the manufacturing the thruster. The final QM will include the most performant solution identified with laboratories model developed at CISAS and KhAI. The QM will be designed according to a thruster optimization and analysis procedure; it will be representative of the real flight hardware..

V. Experimental set-up and development test at CISAS

The main objective of the experimental campaign is to achieve the best source and magnetic nozzle configuration in terms of maximizing the propulsive efficiency. The performances of plasma thruster are deeply affected by several parameter which need to be varied in order to identify the best thruster configuration. To do so the experimental set-up has been designed allowing many degree of freedoms.

The key parameters involved can be classified in the following categories:

- Geometrical parameters: plasma source length, outlet diaphragm diameter, injector shape and dimension;
- Antenna and power network: antenna type and axial position, matching network, feeding frequency;
- Magnetic field: magnetic field intensity and gradients, provided by solenoids or permanent magnets.

The experimental setup is provided by various diagnostic devices in order to perform cross-measurements of the characteristics of the plasma source and of the ejected beam:

- Optical spectrometers, with different operative ranges and resolutions, to estimate electronic temperature and density;
- Microwave interferometer, to evaluate plasma density;
- Retarding potential analyzer (RPA), that can be assembled with different grids configurations, to characterize the energy of theplasma beam;
- CCD cameras with band-pass filters, to identify the ionized region.

In the sub-section A a full description of the experimental setup and diagnostics is given.

In the sub-section B an overview of the development tests and the more significant results currently achieved are presented.

A. CISAS experimental facility

A.1 Experimental setup

Vacuum apparatus.

The hydraulic scheme of the apparatus is shown in Figure 2; valves, pressure sensors and pumps are indicated by apposite abbreviations.

The vacuum apparatus consists of a 2-m length-0.6-m diameter vacuum chamber and a pumping system composed of a *diffusive pump* (D1) and *a turbo-molecular pump* (T1), supported by two auxiliary pumps, a *rotary* (R1) and a *roots* (R2) ones, to guarantee the proper back pressure for the former pumps. The diffusive pump is the best trade-off solution considering the volumetric flow and the cost; moreover it better permits variable operating conditions in comparison with turbo-molecular and cryogenic systems. The reasons of the variable conditions are the prospective fluctuations in the mass flow rate during the experiments and the air re-entries due to the changes in the geometric configuration of the plasma source. However, diffusive pumps can lead to the contamination of the chamber because of the vaporized oils. This problem is minimized using the turbo-molecular pump in parallel with the diffusive pump. A gate valve V8 is mounted at the interface between the plasma source and the vacuum chamber in order to reduce the contamination of the chamber due to the frequent air re-entries. This methodology allows to constantly maintain the vacuum chamber in a high or medium vacuum level, even when the source is disassembled for servicing.

The overall pumping capacity is 12600 L/s.

The vacuum level is measured by means of five *Pirani pressure gauges* (P1, P2, P4, P5, P6), a *high-vacuum Penning gauge* (P3), and a *mass spectrometer* (residual gas analyzer), able to detect ionized molecules with a mass-to-charge ratio up to 300. The last is used to monitor flange leaking and contamination due to pump-oil.

The maximum vacuum level reached without the injection of a mass flow is 5e-7 mbar and the possible presence of contaminants is monitored through a mass spectrometer before each experimental operation. In case of mass flow injection, the vacuum level depends on the mass flow value and the pumping line activated, normally for the mass flow rate used (between 10^{-7} kg/s and $4x10^{-7}$kg/s) is in the range of $10^{-5} – 10^{-4}$ mbar.

The plot reported in Figure 3 shows the trend of the vacuum chamber pressure versus injected mass flow rate both with the diffusive and the turbo-molecular pumps working together and with the sole turbo-molecular pump.
During the experiments both the pumping lines are connected to the vacuum chamber, whereas during stand-by or servicing time only the turbo-molecular is employed.

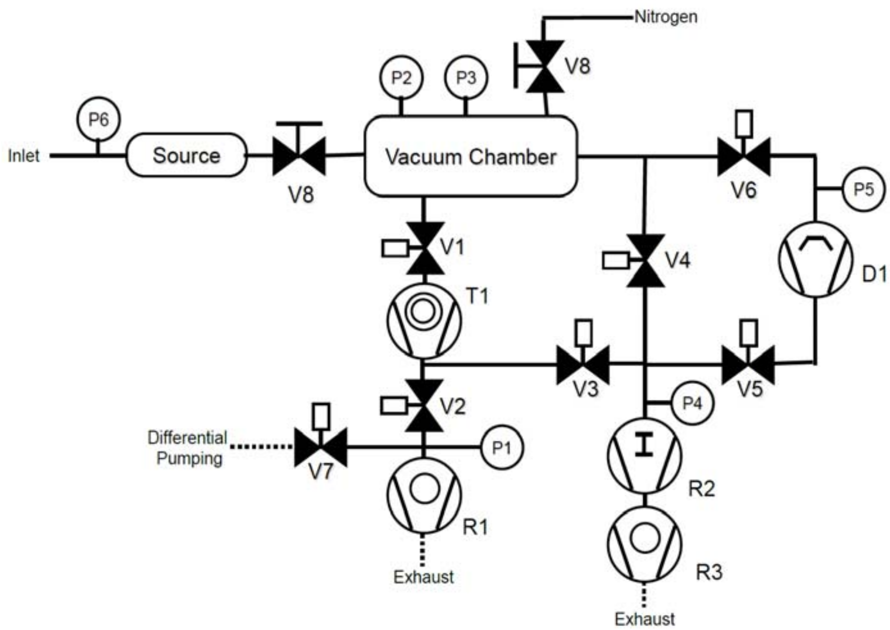

Figure 2. Hydraulic scheme of the vacuum apparatus with valves (V1 to V6 pneumatic ones, V7 manual one), pressure sensors (P1, P2, P4, P5, P6 Pirani ones, P3 Penning one) and pumps (D1, T1, R1, R2, R3)

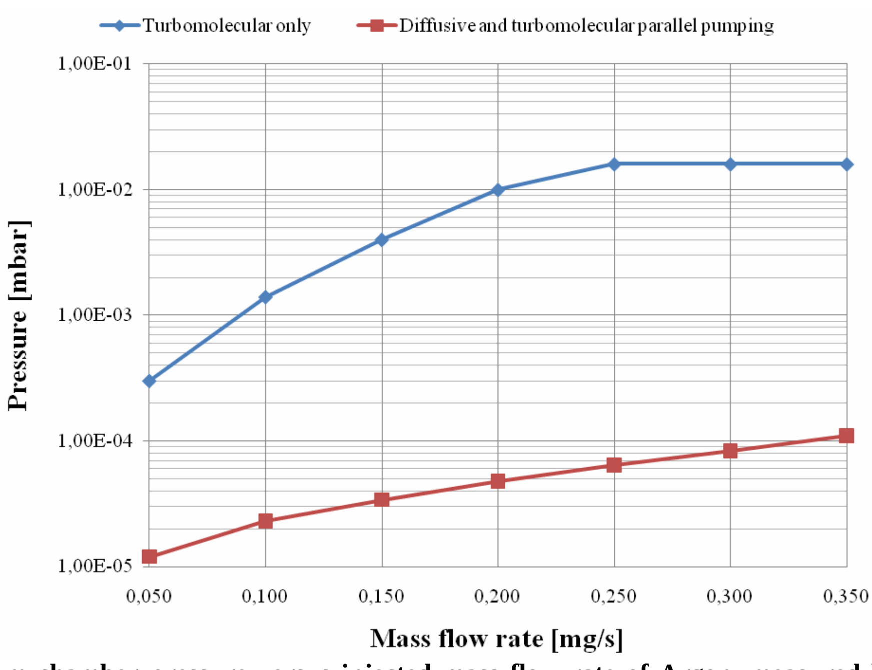

Figure 3. Vacuum chamber pressure versus injected mass flow rate of Argon, measured by means of the combined use of a Pirani gauge and a high-vacuum Penning gauge

Thruster development model lay-out.
The thruster development model is installed outside the vacuum chamber to allow quick modifications of the experimental set-up. The main components are the following:

1) a *pyrex expansion bell* directly linked to the vacuum chamber, where plasma is ejected; this component allows the observation of the plasma beam;
2) a *pyrex tube (i.e.* the *plasma source)* with a inner diameter of 19mm and an outer diameter of 25mm where the plasma is generated;
3) a set of *ceramic outlet diaphragms* that can be changed in order to test different outlet diameters;
4) a *ceramic injector* with a 2mm central axial hole;
5) an *injection system,* responsible of gas feed into the source; a piston mechanism allows to change the source length; the mass flow is regulated through a MKS feedback controller in the range from 0.1 up to 0.4 mg/s with an accuracy of ±(0.008+0.1% rv) mg/s, where rv stands for reading value;
6) an *antenna* for plasma generation, coaxial to the plasma source, and a RF power supply network able to operate at different frequencies;
7) a *permanent magnets* frame, coaxial to the plasma source and axially movable along the source; a brief description is reported below.

Figure 4 shows a picture of the overall assembly of the development model and highlights the main components.

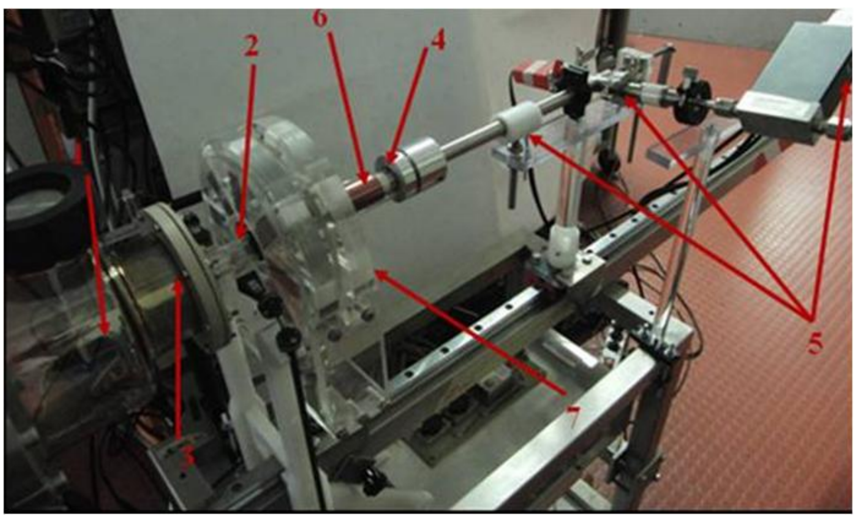

Figure 4. Main components of the thruster development model: 1) pyrex expansion bell; 2) pyrex source (i.e. plasma source); 3) outlet diaphragm; 4) ceramic injector; 5) injection system; 6) antenna; 7) permanent magnets frame. A detailed CAD of the system is reported in Figure 13

Permanent magnets frame.
Different magnetic solutions have been tested, progressively approaching the final model (flight model) of the thruster. The first step was the employment of a system of four solenoids, independently powered, and placed at different axial positions along the source. This system allowed a deep variability of the field in terms of both intensity and shape of the magnetic lines, thanks to the feed current changeability. Subsequently a solution based on permanent magnets have been installed. The design of these magnets lay-outs has been driven by the analysis of the measurements performed during the solenoids system stage.
Currently, the magnetic field is generated by SmCo5 cubic permanent magnets with a size of 20mm. The housings of the magnets consist in a Plexiglas disks with radial grooves where the magnets are located at the proper radial position and held by Teflon spacers (Figure 7). In this way the magnetization vector can be oriented both in the axial and in the radial direction. Moreover the whole frame can be axially translated along the source since it is mounted on a carriage.
Several configurations have been tested; however, the measurements presented in this paper have been obtained employing the magnets lay-out shown in Figure 5 because of its better performances in terms of plasma density and temperature in the source region. The magnetic field is provided by a double ring of axially-oriented-magnets coupled with a ring of radially-oriented ones, following the scheme illustrated in Figure 5. Figure 6 illustrates the magnetic profile on the axis measured by means of a Hall probe. This permanent magnets lay-out produces an

asymmetrical axial field exhibiting a strong (≈1400 G) central peak with two inversion zones and two secondary peaks of different intensity (800 G and 200 G). The peak of 800G is located on the outlet side, whereas the antenna is located on the 200G peak side.

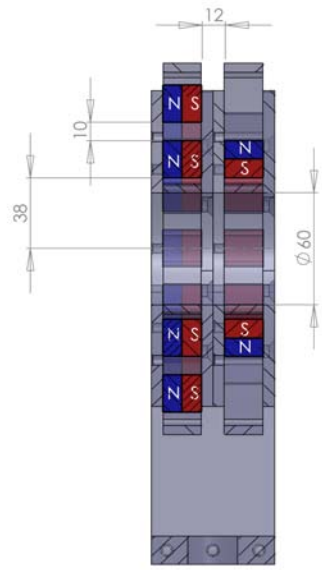

Figure 5. CAD scheme of the permanent magnets lay-out employed for the experiments

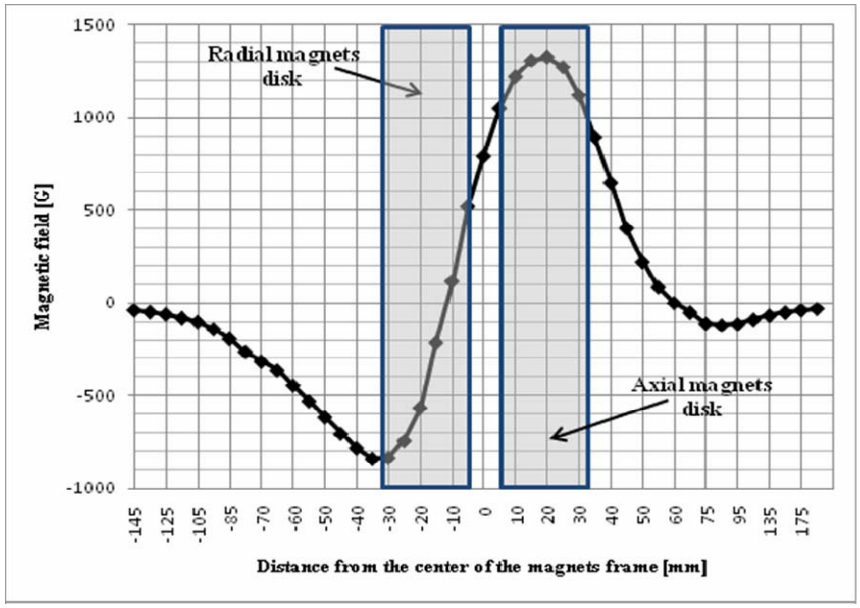

Figure 6. The magnetic field generated by the permanent magnets frame selected, measured by means of an Hall probe. The position of the radial magnets disk and of the axial magnets disk are also displayed

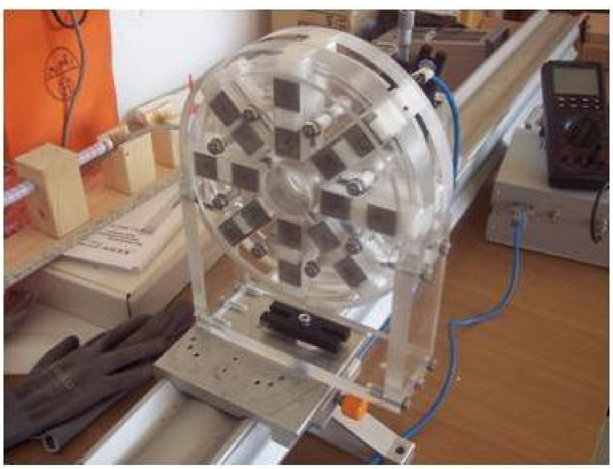

Figure 7. Permanent magnets frame. The cubic permanent magnets are housed in a Plexiglas support with radial grooves

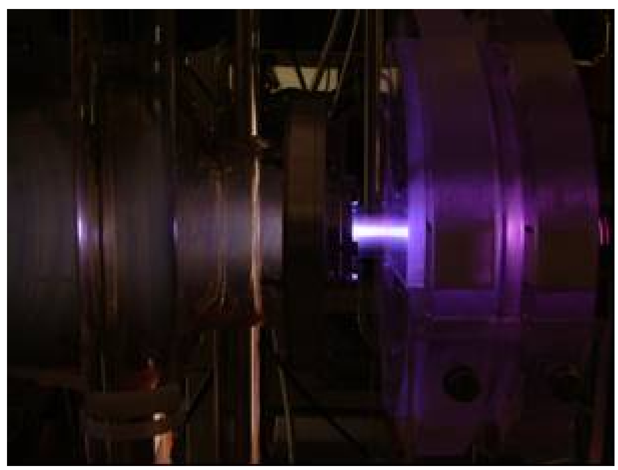

Figure 8. Permanent magnets installed on the development model, during the operational phase. The plasma present a high intensity blue core. On the left side the ejected beam can be observed through the glass bell

A.2 Diagnostic systems

Optical spectrometry

Two optical spectrometers are used to acquire the emission spectrum of the plasma, in order to extrapolate information on the ratios between atomic excitation and ionization as well as on the electronic temperature:

1) an Ocean Optics HR4000 spectrometer, with a wavelength range 380-830nm, a slit width of 25μm and a resolution of 0.54nm;

2) an Ocean Optics HR4000 spectrometer with a wavelength range 220-575nm, a slit width of 5µm and a resolution of 0.24nm.

The coupled employment of these devices allows the observation of a broad band of the emission spectrum from the near UV to the near IR and at the same time to focus on the lower wavelength region where the main ArII lines are present.

Both spectrometers are interfaced to the plasma source by means of an optical fiber, 2m long and with a 600µm core diameter; the optical fiber heads look the same source section, located usually 5mm before the outlet position, and are displaced in order to point the plasma core.

Spectrometers measurements are affected by the presence of the glass tube (i.e. plasma source), which is responsible of a wavelength-dependent attenuation of spectrum intensity; despite this, a rough analysis allows qualitative comparisons between the different configurations tested. For a deep investigation a further elaboration of the acquired data is needed: removal of the environmental noise, matching with the theoretical spectrum and so deducing the wavelength shift, superimposition of the calibration curve which takes into account the glass filtering effect.

The ionization level is evaluated by means of four ArII to ArI lines ratios: 420, 452.2, 355.9, 434.8, 488 nm. The first couple of values corresponds to the argon excitation level while the last three values identify the ionized argon; then the ratios E(355.9)/E(420), E(434.8)/E(420), E(488)/E(420), E(488)/E(452.2) are calculated to trace their dependency on the key parameters. The set of measures gains reliability if all the ratios show an equal trend and this circumstance allows the employment of the ratios to perform a qualitative comparison among different configurations.

It has to be underlined that this kind of spectral analysis is based on the simplifying hypothesis of a plasma in local equilibrium both along the axis and across the section. Nevertheless in a helicon thruster, plasma can't be considered properly homogeneous, stationary and in a LTE condition and this forbids the possibility of directly evaluating n_e and T_e. The lack of a complete LTE condition for the plasma produced at CISAS has been demonstrated by comparing the acquired spectra with those of an Ar hollow cathode near equilibrium[21]. However this does not hamper the possibility of using the aforementioned ratios for qualitative comparisons on the propulsive performances.The estimation of the electronic temperature T_e and the electron density n_e instead is due to Katsonis[21]. To describe this plasma a simplified "global" model and also a detailed PIC one have been used[22]. A C-R model[23] provides the theoretical spectrum to compare line intensities of the main ArI, ArII and ArIII multiplets with, allowing a distinct evaluation of n_e and T_e for the different argon species present. It has to be noticed that the C-R model is a zero-dimensional code. A first estimation of the plasma temperature can be obtained by looking to the relative intensities of the (Ar I) 4*s*-5*p* and (Ar II) 4*s*-4*p* multiplets of the two species. Nevertheless because the optical path encompasses an external cold plasma region, where the abundance of Ar I prevails, therefore the Ar I percentage is overestimated; accordingly, the obtained bulk T_e is lowered. The T_e in the plasma core can be better evaluated from the Ar II / Ar III ratio. The so obtained T_e concerns essentially the central part of the plasma, where the bulk of the Ar II and Ar III amount is concentrated. Unfortunately most of times ArIII lines are hard to identify[21] due to the strong attenuation due to the pyrex glass below 300nm.

Microwave interferometer

The working principle of this instrument lies on the phase difference between a microwave reference signal and a microwave beam which crosses the plasma; this phase shift is due to the plasma effect on the beam itself.

Two microwaves signals at 75GHz and 75.1GHz are generated starting from a 100MHz signal. One of them is driven across the plasma through a couple of radiating/receiving standard gain horns, whereas the reference signal propagates along a waveguide.

The phase difference between the signals driven through the different paths depends on the refractive index of the mean between the two horns, therefore on plasma density. Figure 10 illustrates the phase difference drop due to the powering off of the plasma discharge. This drop is a linear function of the plasma density and, in the assumption of an O mode wave propagation, can be expressed by:

$$\Delta\varphi = \frac{e^2}{4\pi c^2 \varepsilon_o m_e} \lambda \int_0^D n\,dl = 2.82 \times 10^{-15} \lambda D \bar{n} = \frac{1.29°}{10^{17}} \bar{n} \quad (1)$$

where λ is the wavelength, *D* the plasma thickness and $\bar{n}$ the plasma average density (expressed in m^{-3}).

The phase resolution of the interferometer is equal to 0.06°, leading to to a density resolution of $0.5 \cdot 10^{16}$ m^{-3}, for a plasma thickness of 20mm of diameter[24].

Finally, the phase is measured through a low noise digital phase detector with a phase noise of 0.01°. The plasma thickness is estimated by means of a CCD camera.

Figure 9. The microwave interferometer

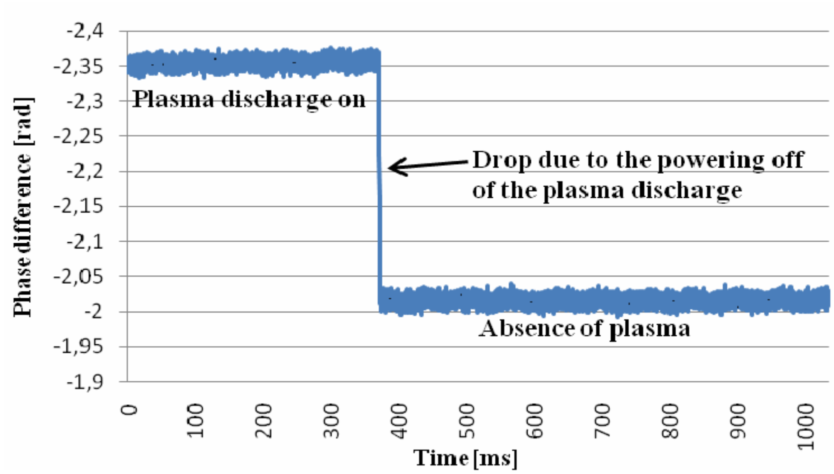

Figure 10. The phase difference drop due to the powering off of the plasma discharge. The value of the drop is a linear function of the plasma density

RPA

The role of the retarding potential analyzer is to evaluate the ion distribution function of the plasma beam and to investigate the prospective presence of multiple populations, allowing the comprehension of their influence on thruster performances. Many configurations have been tried, distinguished by grids number and their polarization and reciprocal distances, in addition to the spacers material.

The chosen configuration is very close to what has been already applied on other experiments[25] and is showed in Figure 11. It presents an assembly of three grids plus the collector placed at different potentials:

1) an outer grounded screen grid G1 to isolate the analyzer from the plasma;
2) a positively polarized grid G2 to energetically discriminate the ions by means of a potential sweep;
3) a grid G3 with a negative potential to repel the unwanted incoming electrons and rebound secondary electrons from the collector; this negative value can be regulated according to the specific intensity of the plasma generated;
4) a collector C to detect the incoming current.

The grids have a circular shape and present a 30μm square mesh of nickel welded between two copper annular supports in a sandwich-like configuration. The central channel presents a diameter of 2mm. The grids are spaced by some ring insulators made of MICA. The spacings between the grids are: 0.4mm between G1 and G2, 0.8mm between G2 and G3, 0.6mm between G3 and the collector. All these components are housed in a peek cylinder to insulate the inner grids from the external case made of stainless steel.

Up to now, the RPA is installed 100mm downstream the outlet diaphragm in a dedicated housing of the glass bell. Future measurements will involve the use of a robotic arm located inside the vacuum chamber, to perform axial and radial scans of the plasma beam.

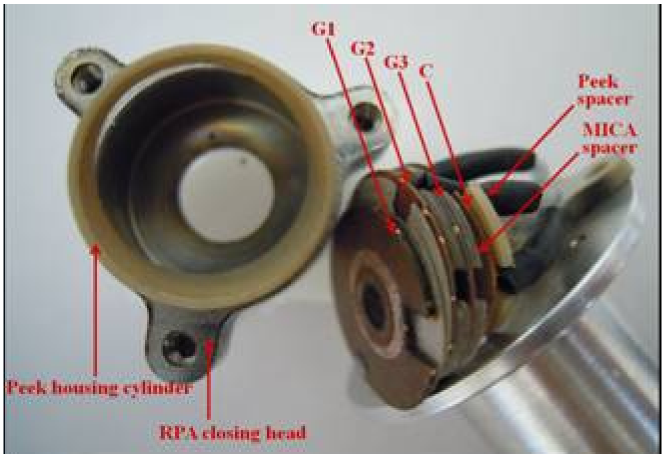

Figure 11. RPA actual configuration

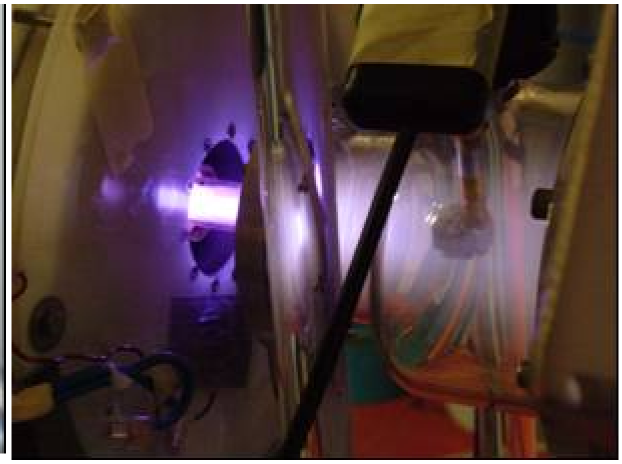
Figure 12. The RPA installed 100mm downstream the outlet in a dedicated housing on the glass bell

<u>CCD cameras</u>
The diagnostics of the experiment include two Basler Sca1400-30FC cameras with a color CCD sensor of 1388x1038 pixels for observation of the plasma in the visible band of the light spectrum. The cameras are employed in combination with lenses and filters whose pass-band is centered on the main ArI and ArII lines to monitor the distribution of ionized and excited particles within the source and the plasma beam.
Two band-pass Omega Optical filters with a band width of 10nm are available for this purpose:
1) a filter with a central wavelength equal to 488nm for ArII detection;
2) a filter with a central wavelength equal to 751nm for ArI detection.

B. CISAS Development tests

In this section the development tests and the main results currently achieved are described. The core of the experimental activity lays on the development and installation of a diagnostic apparatus ready to obtain cross-measurements of the plasma properties. Particularly, the measured plasma characteristics are the following:

- plasma temperature and density into the source obtained by means of spectrometry; in this paper only qualitative trends of the ArII to ArI lines ratios are reported in order to lead a comparative study among the different thruster configurations; a more rigorous analysis, temperature T_e and density estimations are presented by Katsonis et al. in a dedicated paper[21];
- plasma density into the source, estimated by means of the microwave interferometer;
- the ion energy of the ejected beam, measured through the RPA;
- the plasma distribution into the source and the divergence of the beam, detected through CCD cameras in combination with band-pass filters.

This section is structured in three parts:
1) an overview of the experiment, which highlights the experimental test bed degrees of freedom and the test procedure followed (<u>*B.1*</u>);
2) characterization of a plasma source employing a 10 MHz antenna; (<u>*B.2*</u>);
3) comparison between the performances of two antennas (<u>*B.3*</u>).

<u>*B.1 Tests Overview*</u>
Figure 13 illustrates the overall scheme of the experiment, which refers to the system of Figure 4, while Figure 14 presents a detailed view of the source region and the geometrical degrees of freedom.

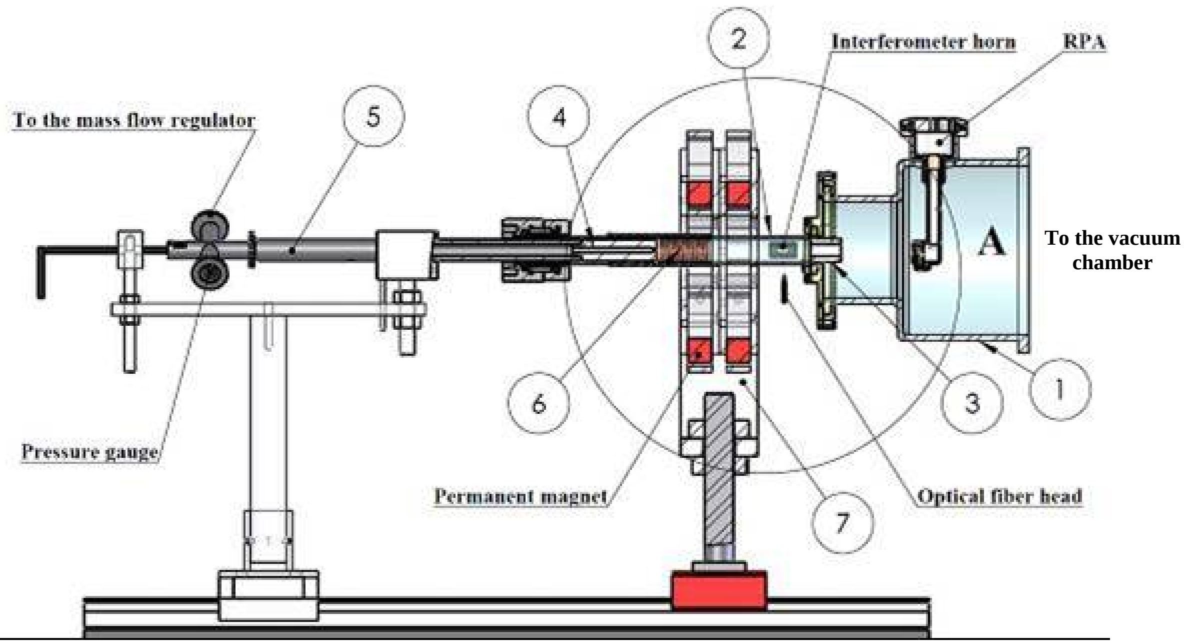

Figure 13. Overall CAD of the experiment and its main components: 1) pyrex expansion bell; 2) pyrex source (i.e. plasma source); 3) outlet diaphragm; 4) ceramic injector; 5) injection system; 6) antenna; 7) permanent magnets frame

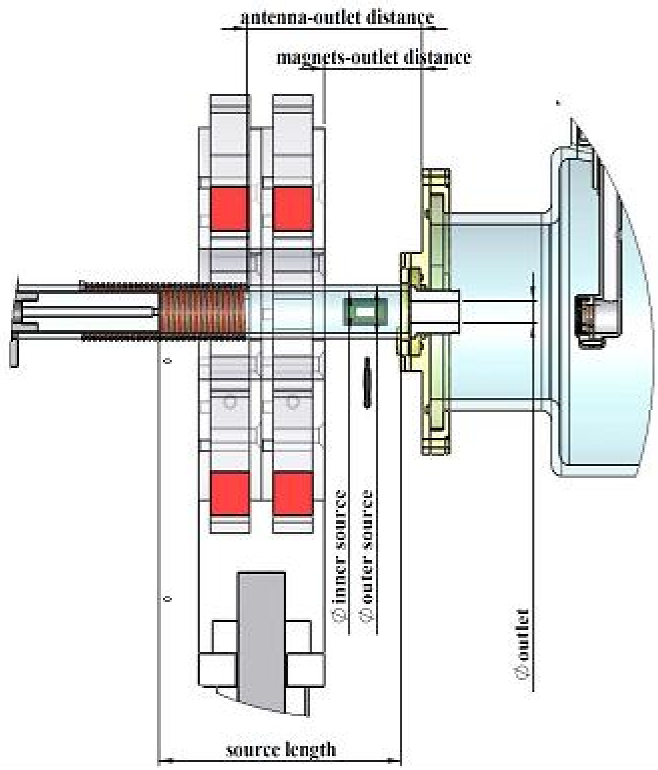

Figure 14. Detailed view of the plasma source region with the main geometrical features highlighted

The free geometrical features are the following:

1) source length;
2) outlet disk diameter;
3) magnets frame axial position;
4) antenna type (i.e. designed to operate at a given feeding frequency);
5) antenna position.

Moreover the following parameters are modulated:

1) power;
2) mass flow rate.

For each experimental sequence, the following procedure has been performed:

1) installation of the outlet disk;
2) installation of the antenna;
3) vacuum creation inside the plasma source;
4) individuation of the optimum value of source length;
5) individuation of the optimum value of the antenna position;
6) individuation of the optimum value of the magnets position;
7) mass flow rate and power scan.

Steps 4, 5 and 6 are performed maximizing plasma density and optimizing the emission spectrum, acting on a single parameter at a time and constantly monitoring the interferometer and spectrometers outputs.

B.2 Characterization tests

B.2.1 Spectrometers and interferometer cross-measurements

As already said, the argon emission spectrum constitutes a prompt tool to roughly estimate the goodness of a plasma operative condition in terms of electron thermal energy.

Figure 15 shows an example of a typical Ar spectrum acquired and elaborated, where lines of ArI (red ones) and ArII (blue ones) can be distinguished in the wavelength region from 290 nm to 650 nm. Sometimes, some ArIII lines can be identified in the region from 320 to 350 nm when the plasma produced is particularly energetic: their intensities are remarkably weaker that those of ArI and ArII, so a conspicuous increase of the spectrometer integration time is needed to achieve a notable size of them even thought this solution may easily cause a loss of information due to the saturation of other lines. The figure highlights the five lines previously described (section A.2, Optical spectrometry) adopted for the ArII to ArI ratios calculations. These lines have been selected as they are easily detectable in the theoretical versus experimental spectrum matching.

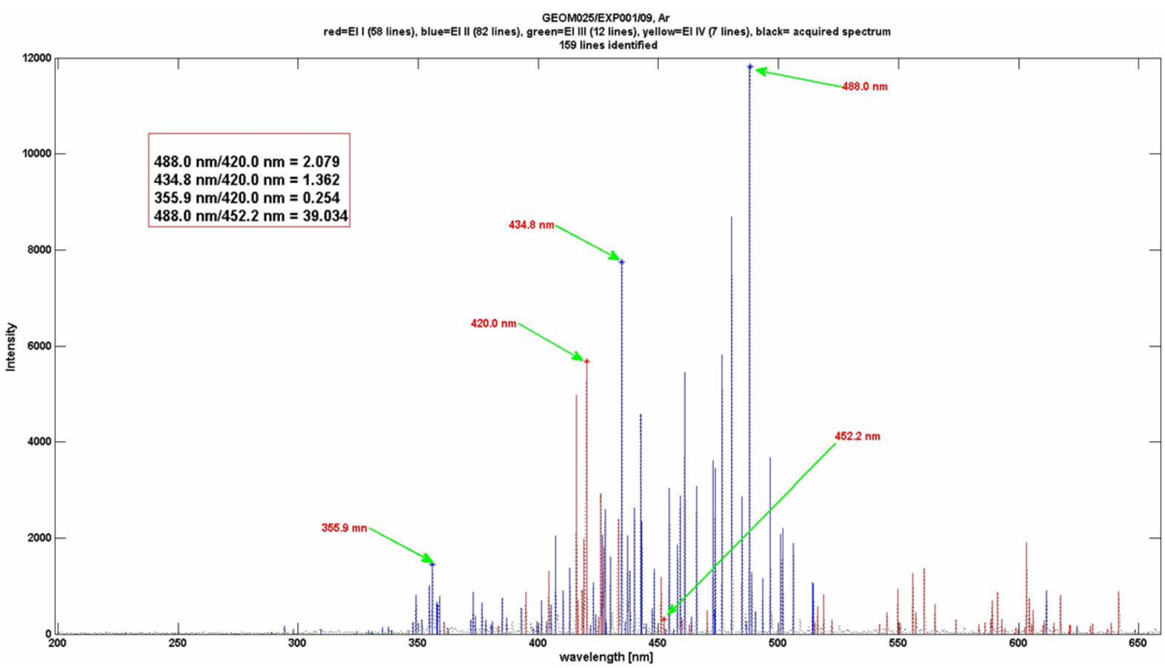

Figure 15. Typical elaborated Argon spectrum; the ArI lines are highligthted in red, ArII lines in blue

Figure 15 reports also the four ArII to ArI ratios aforementioned. For each experimental tests series, an analysis of all these ratios has been a common practice; nonconforming trends can be symptomatic of the presence of spurious data. The following figure (Figure 16) shows, as an example, these four ratios trends obtained for a 10MHz antenna with a source configuration as reported in Table 1.

Parameter	Value
Source length [mm]	135
Magnets-outlet distance [mm]	38
Antenna-outlet distance [mm]	45
Outlet diameter [mm]	5
Power [W]	50
Feeding frequency [MHz]	10

Table 1.

The reported plots display a similar trend for the four ratios, with slight differences on the absolute values. Values are normalized to unity for comparability.

The other geometrical configurations characterized denote a similar response in terms of ratios trends.

As soon as the ratios trends are checked, usually the 488/452.2 nm one is chosen as the reference value.

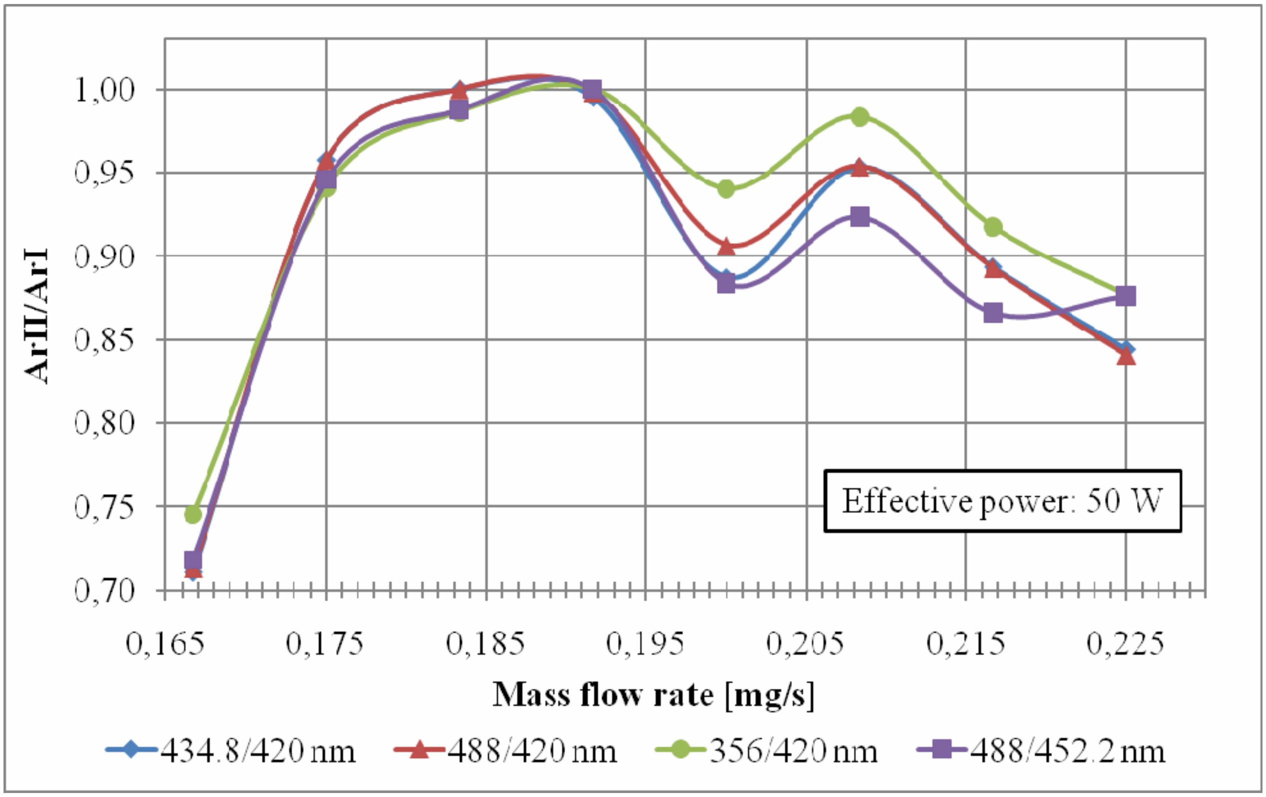

Figure 16. Comparison between the four ArII to ArI ratios

Spectral emission data can be combined with interferometer measurements to get a sense of what is the global performance of the thruster. Broadly speaking, the performance of any thruster can be improved increasing exhaust velocity and mass flow rate; in a plasma thruster, the former is directly dependent from the electron temperature while the latter increases with ions density.

Plasma behavior sensibly changes varying outlet diameter and feeding frequency so it is impossible to deduce general conclusions about spectral emission ratios and density trends as a function of mass flow rate and effective power: each configuration is unrelated to the others.

Hereafter spectrometric (Figure 17) versus interferometric (Figure 18) analysis is reported for a set of measurements performed with the following parameters (Table 2):

Parameter	Value
Source length [mm]	135
Magnets-outlet distance [mm]	38
Antenna-outlet distance [mm]	45
Outlet diameter [mm]	10
Power [W]	50, 65, 75, 90
Feeding frequency [MHz]	10

Table 2.

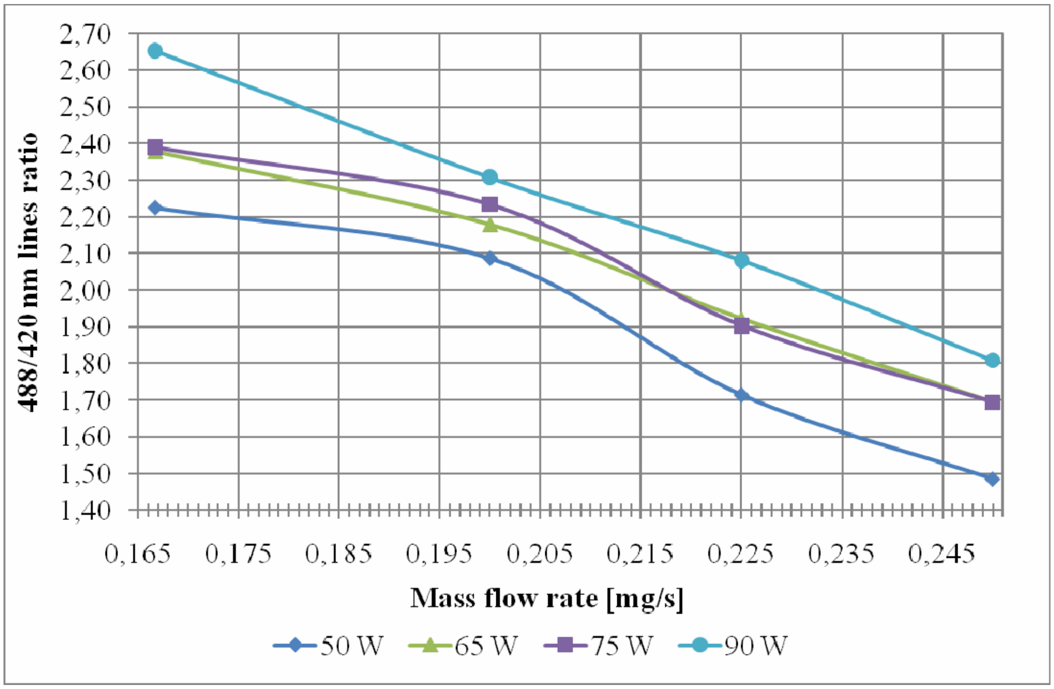

Figure 17. ArII/ArI lines ratio as a function of the mass flow rate for different powers

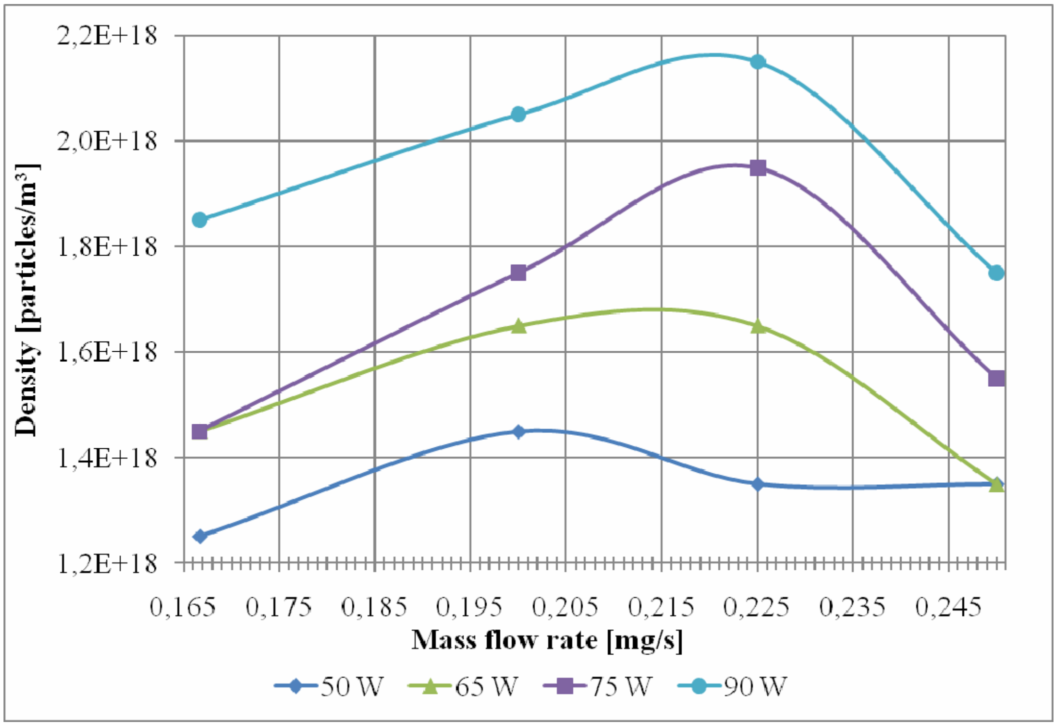

Figure 18. The plasma density as a function of the mass flow rate for different powers

Both the ionization level and the density grow with the effective electrical power but the spectral ratio decreases quite monotonically with the increase of the mass flow rate while the density exhibit a maximum value which does not correspond to the same mass flow rate value for all the power levels.

For a fixed power, this configuration produces a smaller quantity of more energetic ions when the mass flow rate is lower (i.e. 0.166 mg/s), so most of the electrical power goes into temperature rise. As the mass flow rate increases the contribution given to enhance the amount of ions becomes more significant till a maximum is reached. Higher mass flow rates causes a performances fall both in terms of ions density and electronic temperature.

B.2.2 CCD filtered pictures

The CCD cameras have been employed for the visual inspection of the plasma source and the plume inside the expansion bell, with the following purposes:

- to investigate the distribution of ions and excited atoms inside the plasma through the comparison of filtered and unfiltered images of the same zone;
- to observe how the plume inside the expansion chamber is affected by different operating conditions.

An example of source observation by means of the cameras can be seen in figures Figure 19, Figure 20, Figure 21, Figure 22. The operating parameters employed are the following:

Parameter	Value
Source length [mm]	135
Magnets-outlet distance [mm]	35
Antenna-outlet distance [mm]	45
Outlet diameter [mm]	10
Power [W]	60
Feeding frequency [MHz]	10
Mass flow rate [mg/s]	0.15

Table 3.

The first image (Figure 19) shows an unfiltered image of the plasma source, which has been processed with a script to determine the scale of the picture in mm/pixel from a known length (in this case the diameter of the glass tube, 24 mm). The second picture (Figure 20) portraits the same zone using a 488BP10 filter: it can be seen that ions are concentrated in a rather narrow core whose diameter is inferior to the diameter of the whole plasma discharge. A zoom of the area encircled in red is reported in Figure 21, which also shows the estimated diameter of the ionized core. The last figure (Figure 22) reports a contour plot of light intensity inside the discharge, which allows to observe the zones of stronger emission.

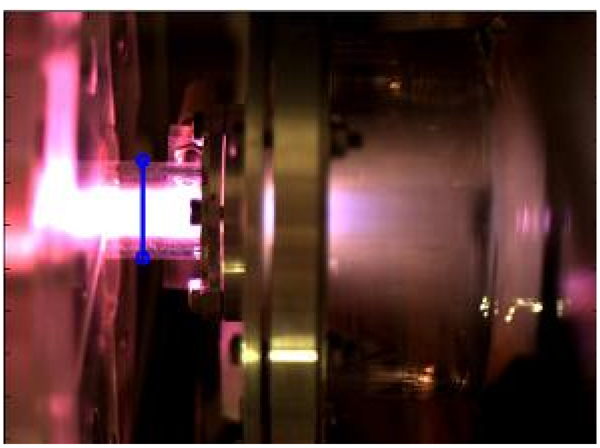

Figure 19. Unfiltered picture of the plasma source; the blue line length is equal to 24mm

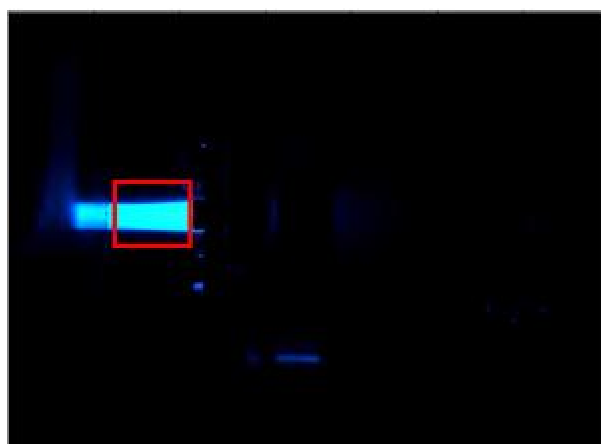

Figure 20. The same picture with a pass-band filter centered on a wavelength of 488nm; the red line contours the region considered for the analysis

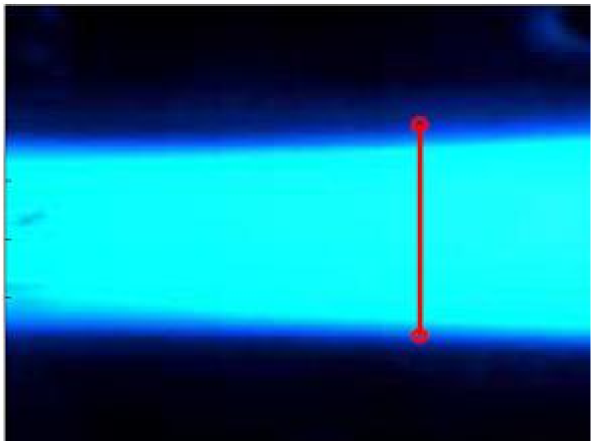

Figure 21. A zoom of the blue core; the red line represents the ionized core diameter

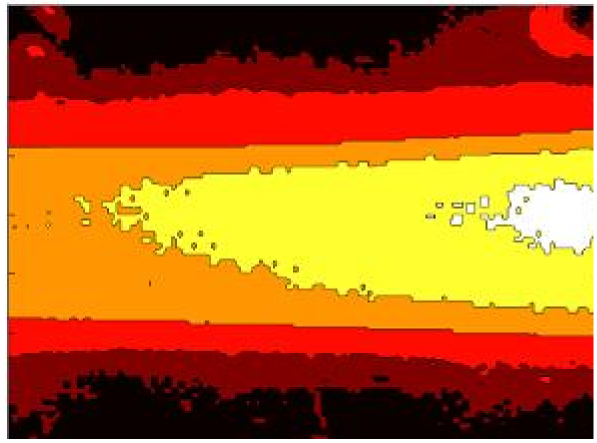

Figure 22. A map of the intensity of plasma emission, which is higher towards the outlet (white color)

The analysis of these pictures has produced the following results:

Parameter	Scale
Picture scale [mm/pixel]	0.105
Ionized core diameter [mm]	7.55

Table 4.

The sequence of pictures from Figure 23 to Figure 26 allows to observe the effect of different input power and mass flow rate on the ejected plume for a given source geometry; the observations have been made employing the system configuration reported in Table 5.:

Parameter	Value
Source length [mm]	125
Magnets-outlet distance [mm]	18
Antenna-outlet distance [mm]	33
Outlet diameter [mm]	10
Power [W]	30, 60
Feeding frequency [MHz]	10
Mass flow rate [mg/s]	0.20, 0.24

Table 5.

It can be seen that the plume presents an ionized core which becomes wider and more extended as power and mass flow rate increased; while the beam divergence does not seem to be appreciably affected by these two parameters, being more related to the magnets position.

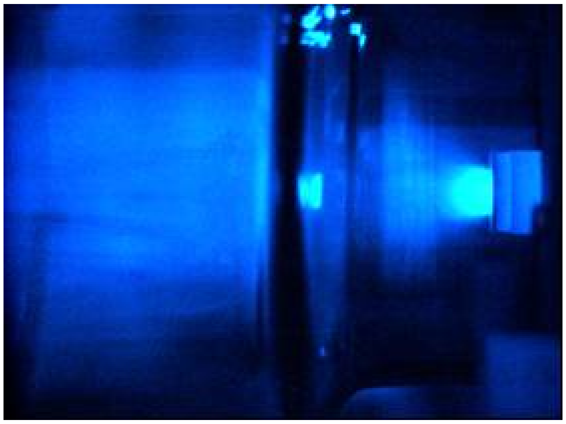

Figure 23. Plasma plume for 0.20mg/s and 30W

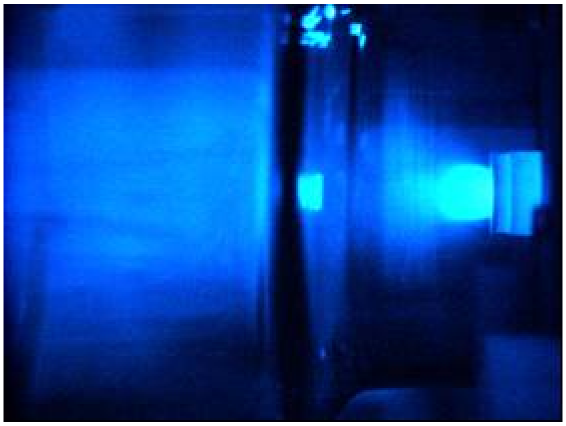

Figure 24. Plasma plume for 0.20mg/s and 60W

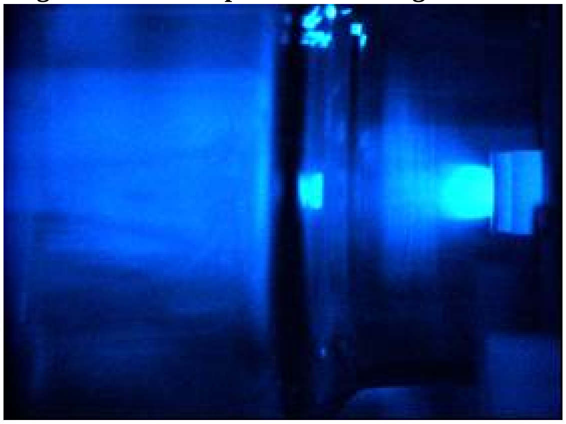

Figure 25. Plasma plume for 0.24mg/s and 30W

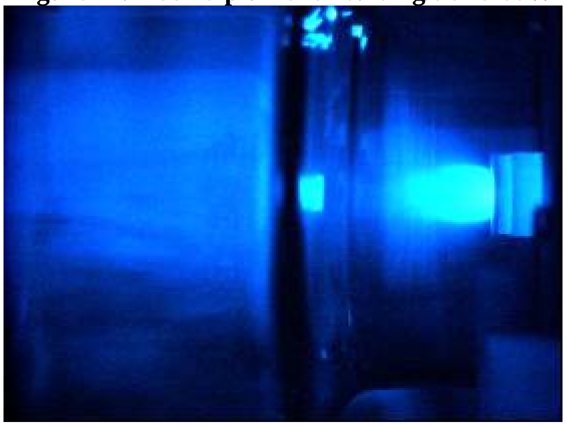

Figure 26. Plasma plume for 0.24mg/s and 60W

B.2.3 RPA measurements

The RPA measurements present a key role in the determination of thruster performance, particularly on the specific impulse. Indeed, the knowledge of the energetic level of the ejected plasma beam allows a rough estimation of the aforementioned parameter in the hypothesis that the detected energy is representative of axial kinetic energy of ions. The RPA is located 100mm downstream the outlet where the acceleration and the detachment stages are fully accomplished. Indeed the acceleration is led by the combined effect of the following phenomena: the potential drop due to the density drop at the interface between the source and the expansion bell, the divergence of the magnetic field which shape the magnetic nozzle. The latter occurs in the region closer to the outlet diaphragm because of the strong decreasing magnetic profile. The steep weakening of the magnetic field magnitude leads also to the immediate detachment of particles.

The presented measurements are obtained for a 10MHz antenna and a source geometrical configuration reported in the table below (Table 6.) .

Parameter	**Value**
Source length [mm]	130
Magnets-outlet distance [mm]	30
Antenna-outlet distance [mm]	50
Outlet diameter [mm]	10
Power [W]	50, 75, 100
Feeding frequency [MHz]	10

Table 6.

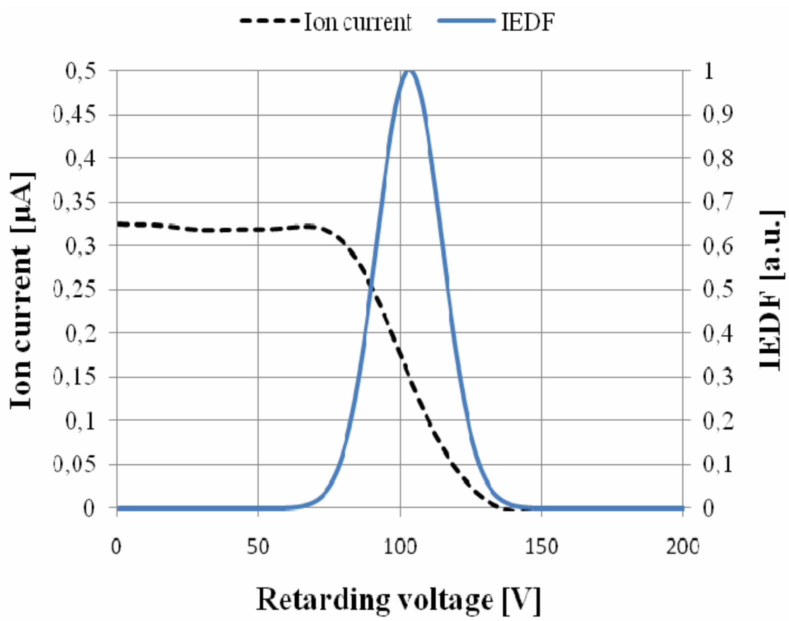

Figure 27. RPA characteristic curve: collected ion current versus the retarding voltage; the estimated IEDF is superimposed

The RPA characteristic curve, namely the collected ion current in function of the retarding voltage, has been acquired for different operative conditions in terms of mass flow rate and power. The signal coming from the DAQ is numerically low-pass filtered to reduce the high frequency noise. Subsequently the first derivative of the curve is calculated employing a five point stencil method and fitted through a Gaussian function in order to represent the ion energy distribution function (IEDF). Figure 26 illustrates the characteristic curve relative to a mass flow rate of 0.2mg/s and a power equal to 100W, together with the estimated IEDF. The curve reveals a strong acceleration mechanism with the energy peak for a retarding voltage higher than 100V. However this voltage is biased by the plasma potential that should be subtracted to the read value.

The trend of energy and ion current in function of the mass flow rate is apparent from the observation of the plots shown in Figure 28 and Figure 29: both decrease for an increasing mass flow rate at the same power level. These results suggest that lower mass flow rates lead to higher ionization level and temperature with a remarkable efficiency in terms of power transfer from electromagnetic waves to plasma. On the contrary, for high mass flow rates the global performances of the source decrease. This effect is in agreement with the spectra acquired for this source configuration and previously displayed (section B.2.1).
Finally, the profiles reported in Figure 28 and Figure 29 highlight the overall increase of the ion current and energy for an increasing power; indeed an additional supplied power drives the heating process.
As previously quoted, the detected ion energy is representative of the kinetic energy of the beam and allows to roughly evaluate the ejection velocity.

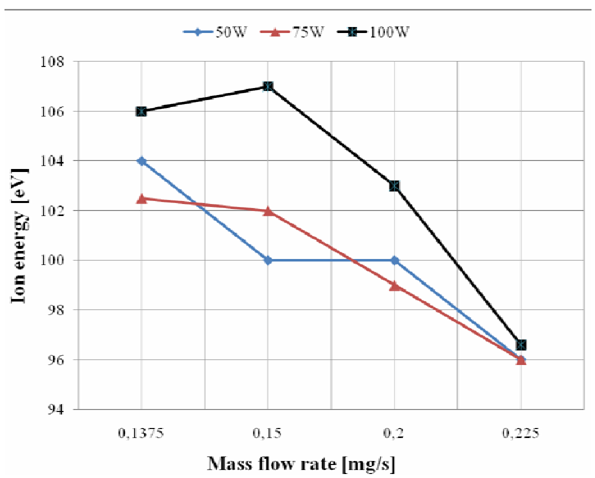

Figure 28. The ion energy as a function of the mass flow rate determined by means of a RPA

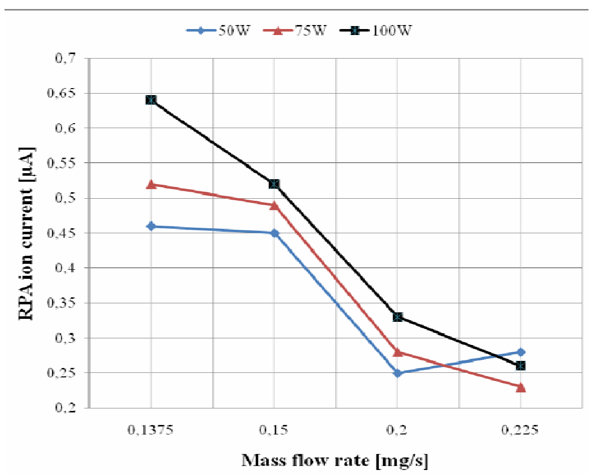

Figure 29. The ion current collected by the RPA as a function of the mass flow rate for different powers

B.3 Data comparison

B.3.1 Influence of the outlet diameter

This section reports the performance of two plasma sources, employing different antennas, each one tested with different outlet diameters. The parameters used in these tests are the following:

Parameter	Antenna 1	Antenna 2
Source length [mm]	145	135
Magnets-outlet distance [mm]	40	38
Antenna-outlet distance [mm]	55	45
Outlet diameter [mm]	5, 10	5, 10, 15
Power [W]	50	50
Feeding frequency [MHz]	3	10
Mass flow rate [mg/s]	From 0.167 to 0.250	From 0.167 to 0.250

Table 7.

The performance of the antennas has been analyzed in terms of plasma density and spectral emission.
The effect of the different outlets on antenna 1 is shown in Figure 30 and Figure 31, in terms of plasma density and ArII/ArI lines intensity ratios respectively.

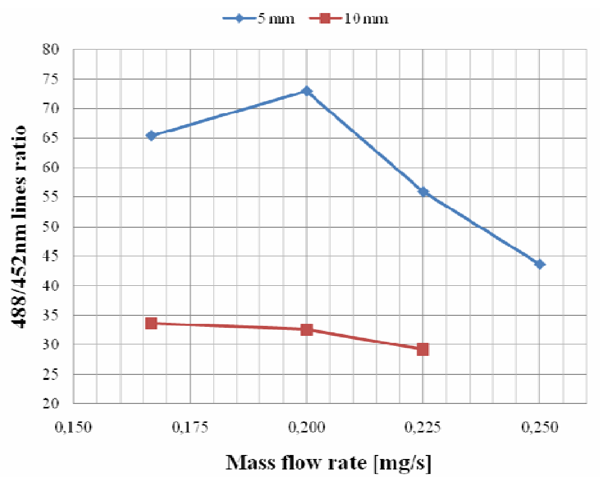

Figure 30. ArII /ArI lines ratio as a function of the mass flow rate for two different outlet diameters, a fixed power equal to 50W, and an antenna designed for a feeding frequency of 3MHz

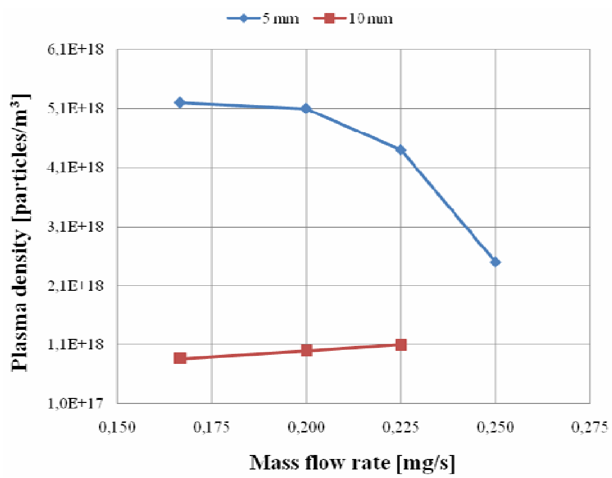

Figure 31. Plasma density as a function of the mass flow rate for two different outlet diameters, a fixed power equal to 50W, and an antenna designed for a feeding frequency of 3MHz

The plasma becomes progressively colder and less dense for increasing mass flow rate in the case of 5 mm outlet; with the bigger one the plasma still gets colder, but its density increases with mass flow rate, thus inverting the previous trend.
A slightly different behavior can be seen in Figure 32 and Figure 33 which show the effects of various outlet diameters on the performance of antenna 2; again the plasma becomes progressively colder with increasing mass flow rate, but in all cases its density exhibits a maximum for a specific mass flow rate whose value depends on the outlet diameter.

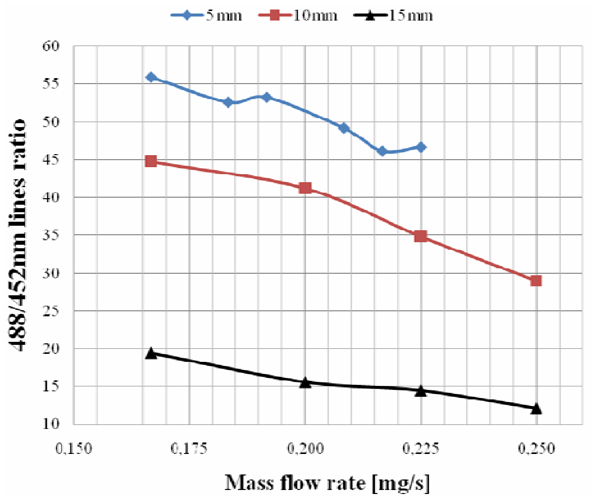

Figure 32. ArII /ArI lines ratio as a function of the mass flow rate for two different outlet diameters, a fixed power equal to 50W, and an antenna designed for a feeding frequency of 10MHz

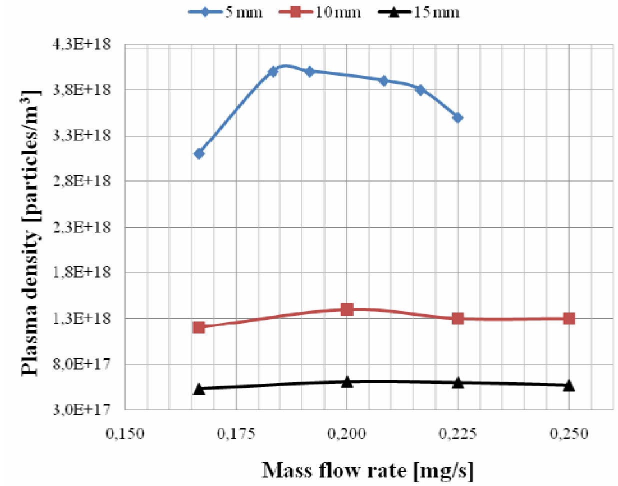

Figure 33. Plasma density as a function of the mass flow rate for two different outlet diameters, a fixed power equal to 50W, and an antenna designed for a feeding frequency of 10MHz

In addion to the aforementioned observations, it has been noticed that an increase of outlet diameter lowers the minimum mass flow rate at which the plasma discharge can be sustained.

B.3.2 Influence of the feeding frequency

The influence of this parameter has been tested comparing the performance of the various developed antennas. This section reports the comparison between the two most performing ones, operated with the same input power and outlet diameter, for a given range of mass flow rates. The other geometrical parameters have been determined for each antenna as explained in section *B.1*.

The employed parameters are reported in Table 8.

Parameter	Antenna 1	Antenna 2
Source length [mm]	145	135
Magnets-outlet distance [mm]	40	38
Antenna-outlet distance [mm]	55	45
Outlet diameter [mm]	5	5
Power [W]	50	50
Feeding frequency [MHz]	3	10
Mass flow rate [mg/s]	From 0.167 to 0.250	From 0.167 to 0.225

Table 8.

The comparison has been carried out considering the obtained plasma density and emission spectrum. The first parameter is reported in Figure 34 as a function of mass flow rate: in the considered range of mass flow rate, antenna 1 generates a considerably denser plasma than the other one. The trend of density is slightly different between the two antennas, with density decreasing monotonically with mass flow rate for antenna 1 and exhibiting a maximum for antenna 2.

The emission spectrum is considered in terms of the 488/452.2 nm lines intensity ratio, whose trend versus mass flow rate is plotted in Figure 35 for the two antennas. Antenna 1 generates higher ratios, which is an index of higher ionization level and electronic temperature. The trends of the ratios versus mass flow rate are similar, exhibiting in both cases a maximum.

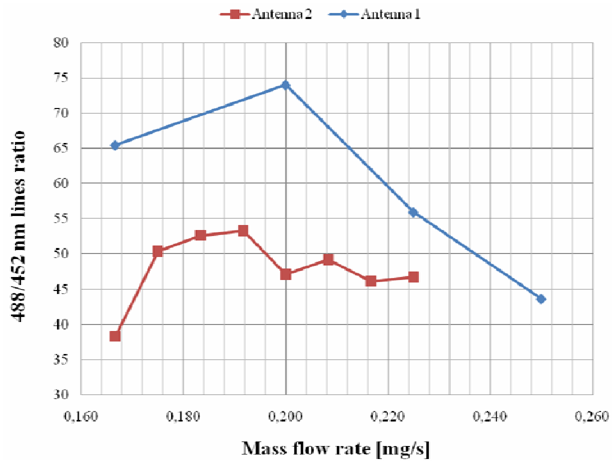

Figure 34. ArII /ArI lines ratio as a function of the mass flow rate for two different antennas, a fixed power equal to 50W, and an outlet of 5mm

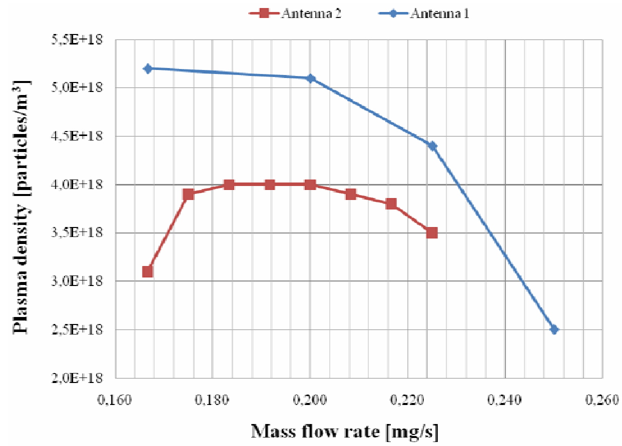

Figure 35. Plasma density as a function of the mass flow rate for two different antennas, a fixed power equal to 50W, and an outlet of 5mm

The reported results show that, for the given outlet diameter and input power, a decrease in the feeding frequency produces an improvement in the performance of the plasma; this is coupled with a general improvement of electrical efficiency thanks to a decrease in magnitude of the parasitic parameters in the power network.

VI. Experimental set-up and development test at KhAI

The research activity done at KhAI includes development, manufacturing and testing of a thruster laboratory models, development and manufacturing of a thruster engineering models (EM) equipped with permanent magnet electro analogs (PMEA), implementation of thermal and magnetic models of the thruster, testing of EM and final the development of the qualification model (QM).

A. KhAI experimental set-up

Investigation activities were carried out on a vacuum stand of the Scientific-Technical Center of Space Power and Engines KhAI. Stand equipment includes single probes set, multigrids probes (RPA) set, spectrometer and balance thrustmeter.

Gas storage and feeding system and power supply system for helicon plasma thruster investigation are shown on figure 36 (left and right respectively).

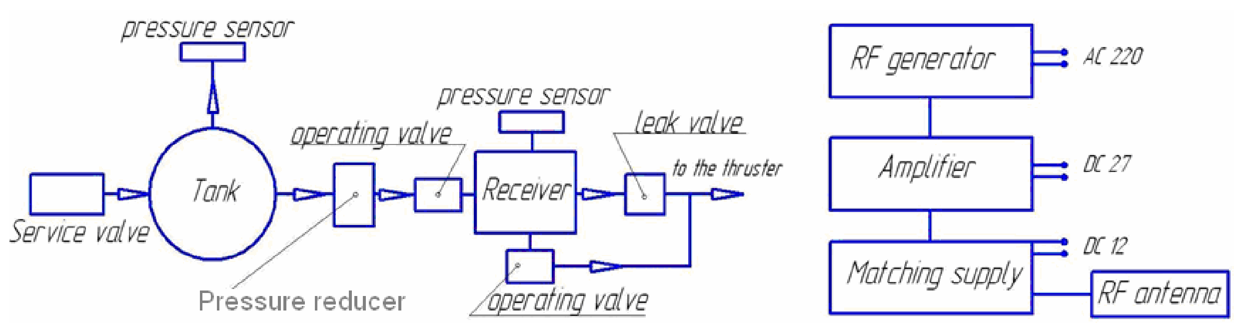

Figure 36. Gas storage, feeding and power supply system's schemes for helicon plasma thruster development

Power supply system consists of RF generator, amplifier and matching box. Cable type – coaxial 50 Ohm. The RF amplifier was manufactured internally at KhAI. A discrete matching box MFJ-993B and MFJ-943E were used in experiments. Working frequency for all experiments has been 13,56 MHz.

Argon was always used as feeding gas. Gas storage and feeding system was made in KhAI. Mass flow rate was regulated from 0,05 to 5 mg/s with accuracy 0,01 mg/s.

Spiral antennas with four and six turns were used in all the experiments. Discharge chamber diameter of laboratory and engineering models is 18 mm. Material of discharge chamber is quartz glass. Discharge chamber length was varied from 40 to 140 mm for different experiments. Diameter of hole in exit ceramic diaphragm (see figure 2) is 4 mm.

B. KhAI Development tests

Laboratory model scheme and photos of experiments are shown on figure 37. Experiments with laboratory models include experiments without and with outer magnetic field. Outer magnetic field was generated by electromagnets and PMEA, which were developed in KhAI and allow to generate magnetic field configuration of permanent magnet with capability change in real time the magnetic field intensity.

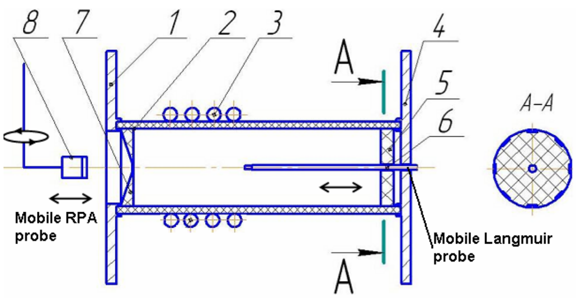

1. End-support flange coupled to the vacuum chamber; 2. discharge tube; 3. RF antenna; 4. external flange;5. ceramic gas-distribution flange; 6. 1/2 coordinate motion inside/outside discharge chamber Langmuir probe; 7. exit ceramic diaphragm; 8. 3 coordinate motion RPA analyzer.

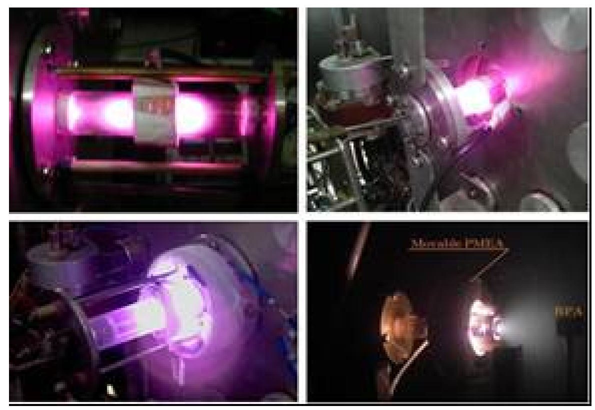

Figure 37. Laboratory model scheme (left) and photos of experiments with laboratory models (right)

In order to identify the best magnetic field configuration based on permanent magnet, several Permanent Magnet Electro-Analogous (PMEA) coils have been developed. Their magnetic field topology is close to the topology of an axially magnetized permanent magnet but instead they allow variation of magnetic field intensity as standard coils. PMEA allow a very important degree of freedom in thruster development since they make it possible to indentify for every thruster configuration the best magnetic field configuration.

Results of magnetic field modeling of electromagnet and for PMEA are presented in figure 38 for comparison.

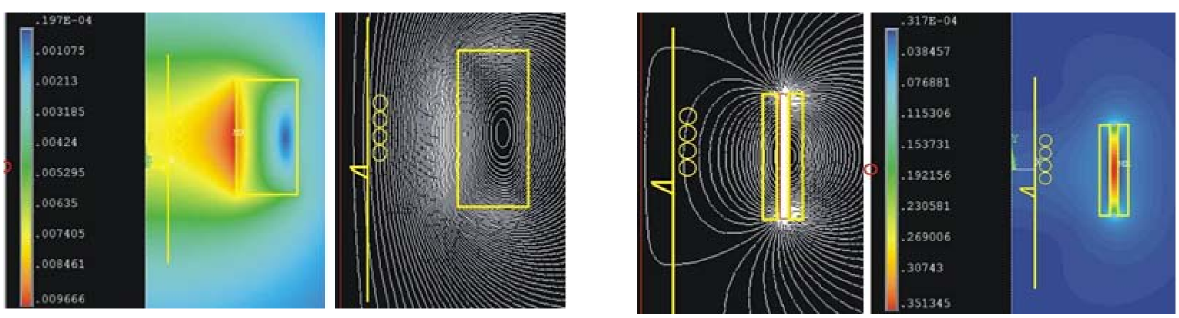

Figure 38. Magnetic inductance and magnetic force lines distributions for electromagnet (left) and PMEA (right)

PMEA has been manufactured to generate magnetic field up to 600 Gauss. In the final version the thruster it will be equipped only with permanent magnets.

The following conclusions were done as results of experiments with laboratory models of the thruster:

1. Two operating modes on Ar with RF power level up to 60 W were registered and investigated: low and high intensity. The most effective for thrust mode operation is high intensity mode which is characterized by significantly higher plasma density than the low intensity mode. This mode is achieved with a special magnetic field configuration discussed in the following.

2. Two electrons populations (1-3 eV and 10-25 eV) have been identified as results of plasma parameters measured by a single Lengmuir probe. RPA plume characterization showed occurrence of one and a double peaks ion energy distribution functions (IEDF). The average ion energy value range from 40 to 180 eV. The value of the average ion energy and the number of peaks of the IEDF depends from the configuration of the magnetic field topology and value.

IEDF of different experiments are shown on figure 39. Applied magnetic fields for demonstrated results were less than 150 G.

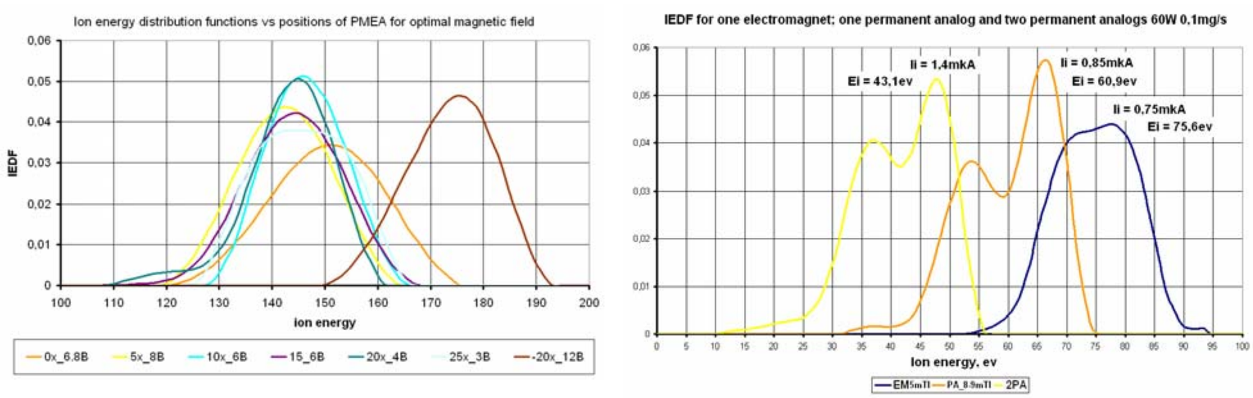

Figure 39. IEDF for different PMEA position relative to nozzle (left) and IEDF comparison for models with electromagnet, one and two PMEA (right)

3. The optimal mass flow rate depends of outer magnetic field configuration and RF power level absorbed by plasma. For magnetic field less than 400 G and RF power level up to 60 W the optimal mass flow rate is in the range 0,06..0,2 mg/s.

4. Based on experimental results and simulations the optimal magnetic field configuration is showed in figure 40. It is characterized by one inversion and a sharp divergence in the antenna zone.

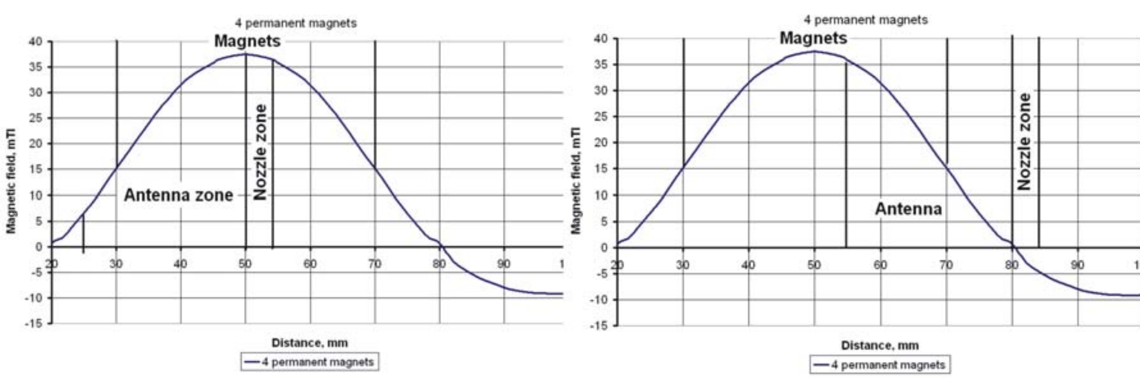

Figure 40. Magnetic field distributions along the axis for two optimal magnetic field configurations.

A jump of about a factor of 10 in the plasma density have been measured from a non optimal magnetic field configuration to the optimal one.

5. Based on the experimental data the expected performances for a 60 W helicon thruster are in the following range: specific impulse up to 2000 s, ionization rate more than 90 % and RF power absorption efficiency up to 80 %.

Based on the experimental results achieved with the laboratory model at KhAI two EM of thruster were developed and manufactured (figure 41). The antenna is a six turns spiral. The mass of second EM with three permanent magnets is 420 g. The discharge chamber length of both EM is 55 mm, the diameter is 18 mm. The nozzle hole is 4 mm.

Figure 41. Photos of EM 01 without case (left) and EM 02 with case and permanent magnets set (right)

i

EM did undergo the following test campaign: (i) at first a thermal characterization of the EM were carried by three thermocouples without PMEA in order to identify thermal influence of separate heat source, (ii) after that the exit plume parameters were measured by RPA with different outer magnetic field configurations generated by PMEA, (iii) finally the thrust provided by the EM will be measured.

The Results of thermal measurements and thermal modeling of EM are shown on figure 42.

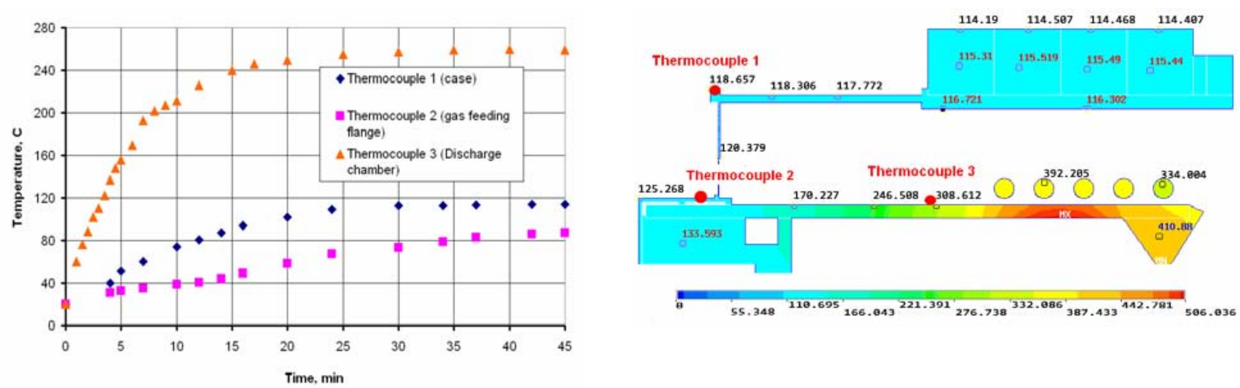

Figure 42. Experimental and theoretical thermal investigation results

Based on the experimental results the predicted temperatures of thruster elements for RF power level up to 60 W are: discharge chamber up to 400 °C, external case up to 120 °C, gas feeding flange up to 90-120 °C, thermal equilibrium operating time 45 min.

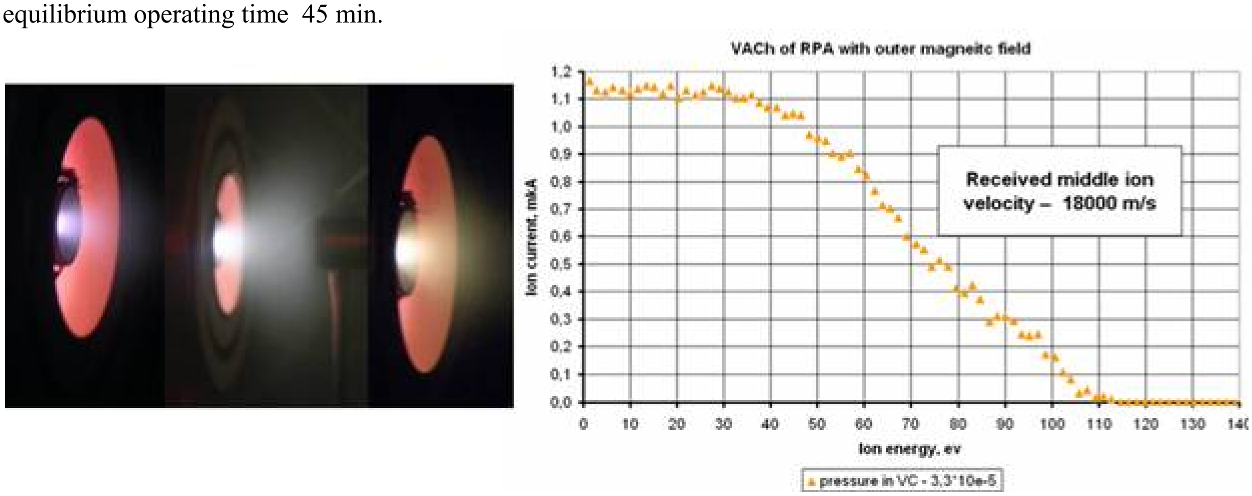

Figure 43. Photos of EM 01 testing and obtained RPA characteristic

RPA scans were carried out to find the optimal magnetic field configuration for EM on the basis of ion current and energy values. RPA curves obtained during EM testing for an optimized magnetic field is shown on figure 43. Calculated middle ion velocity is near 18000 m/s.

At first thrust measurements of EM were planned to be done installing the thruster on a balancestand.. But during gauging of the thrust balance a special effect was registered. Electromagnetic forces, generated by RF current goes through coaxial feeding cable, providing a significant influence on thrust measurements.. Therefore the solution to provide thrust measurements by reverse method (ballistic pendulum) was followed (figure 44). EM was mounted on a fixed supporting arm. Molybdenum plate was fixed and balanced on the thrust meter at the distance 5,5 cm from EM nozzle.

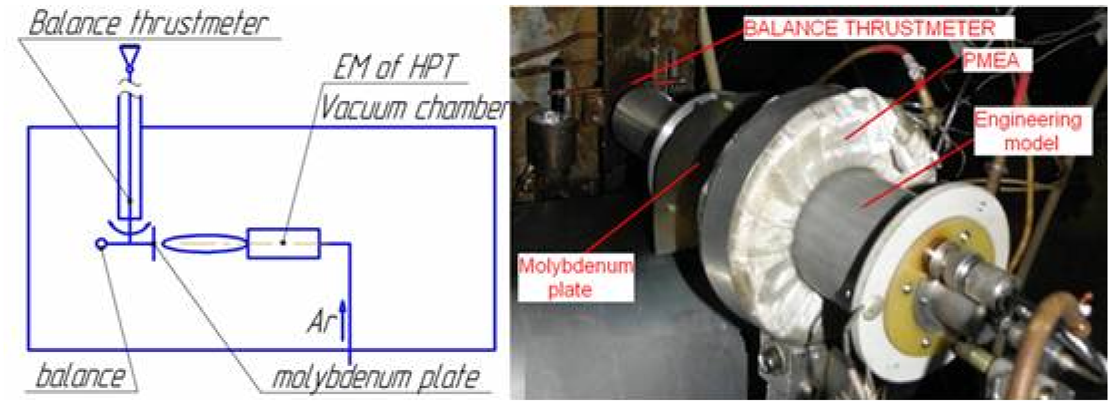

Figure 44. Scheme of reverse method thrust measuring experiment and photo of experiment set-up

At that moment thrust measurements on the EM are still ongoing. To identify proper correlation coefficients between direct and reverse method an SPT thruster will be used as a reference . Today a new vacuum version of RF amplifier is under manufacturing in KhAI. When RF amplifier will be finished it will allow direct thrust measurements.

At the first half of July 2011 EM 02 with PMEA and four permanent magnets set was delegated to ONERA, France for further testing.

VII. Experimental set-up and development test at ONERA

The thrusters will be tested at the Onera Micronewton Facility in Palaiseau (France). The experimental setup is described below.

A. ONERA vacuum facility

The B09 vacuum tank used is optimized for micronewton thruster measurements (Figure 45). The tank is 80 cm in diameter and 2 meters long. It features three Pfeiffer HiPace 2300 turbopumps with 2000 l/s air pumping rate each, for a total of 6000 l/s of clean vacuum. The forepump is a Alcatel 2100 dual stage rotary vane pump (100 m^3/h pumping speed, 3.10^{-3} mbar limit vacuum). The tank is fitted with many electric feedthroughs: low voltage, high voltage (20kV), high current (200A) and coaxial (BNC, SMA and N, floating and grounded). It is also fitted with multiple fluid feedthroughs, optical fiber feedthroughs and optical ports. It is installed on a concrete structure to avoid vibrations during micronewton thrust measurements.

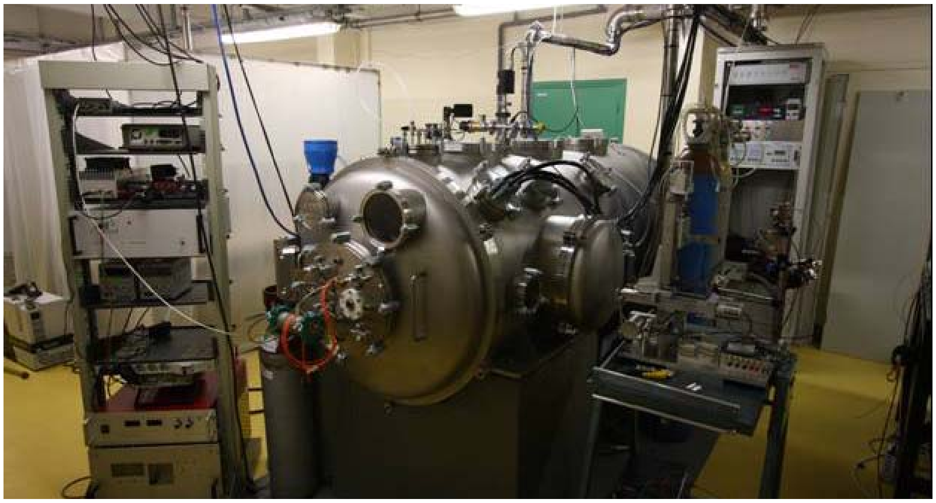

Figure 45. Micronewton facility at Onera.

C. Diagnostics development

Four diagnostics were specifically developed in the framework of this project, and will be applied to the thrusters: RPA measurements, ion mass-energy analysis, 3D Doppler LIF and direct thrust measurements on a micronewton balance.

Retarding Potential Analyzer:

A classical four-grid retarding potential analyzer[26] is used to measure the ion energy distribution function (IEDF) in the plume. The plasma-facing grid can be either grounded or floating. The grid mesh transparency is 50%, yielding a 6.2 % total transparency. A Keithley picoameter is used to measure the ion current collected by the device. The measurement procedure is computer-controlled. The analyzer voltage is varied between 0 and 300 V (Figure 46). Several IV curves are taken and averaged to enhance the signal to noise ratio and thus obtain smoother data for the derivation of the IEDF.

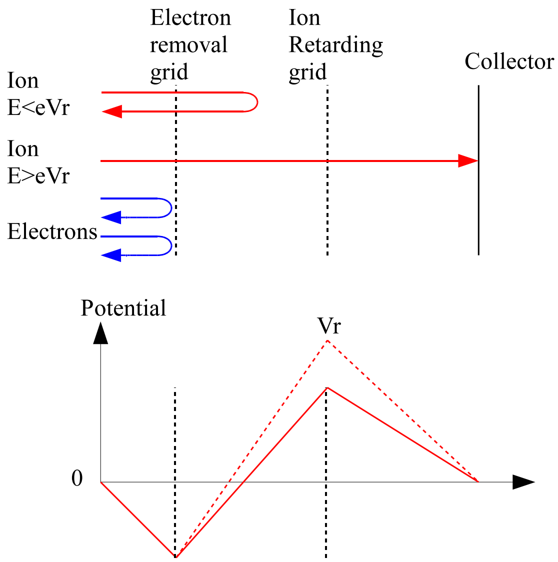

Figure 46. Schematic of the operation of the RPA.

Ion mass energy analysis:

A Hiden PSM ion analyzer is used for the project It allows to make simultaneous scans of mass and energy of the plume. The characteristics are the following:

Mass range: 0-300 amu
Energy range: 0-1000 eV
Energy resolution: 0.5 eV

Laser Induced Fluorescence:

Using a tunable, single mode diode laser, Laser Induced Fluorescence (LIF) will be performed on the plume of the thruster. Several Ar and Ar+ transitions may be used: 852 nm, 773 nm, 668 nm. The tunability allows measuring the mean Doppler shift of Argon along the laser axis at the measurement point (about 1 mm in size). By using three laser beams looking at the same measurement point in the plume, one can deduce the velocity vector. And by scanning the plume one gets the 3D distribution of velocity vectors for both Ar and Ar+.

Practically, the thruster will be mounted on X-Y-Z translation stage and the optics will be fixed. The setup design is based on a previous setup (still existing at Onera) that was used to measure optically the mass flow rate of neutral cesium in a cesium FEEP thruster using 3D Doppler LIF.

Micronewton balance

A dedicated balance will be built based on the current micronewton balance at Onera, which has been successful in measuring thrust down to 0.1µN with cold gas thrusters.

D. Experimental setups

For the application of the diagnostics, two setups will be used:

- a beam scanning setup
- a LIF setup
- the micronewton balance (currently in design phase)

Beam scanning setup

The setup is shown in Figure 47. The thruster is mounted on a rotation stage so that the thruster exit is at the center of the vacuum tank and on the rotation axis. Two diagnostics can be applied with varying angle: RPA (which is placed in the vacuum tank 50 cm away) and ion analyzer (at the other end of the vacuum tank 2 meters away). The angular resolution is a fraction of a degree. A third diagnostics is used at the same time: emission spectroscopy. A 1 inch diameter fused silica lens is mounted on two small, piezo translation stages below the thruster, and an optical fiber is used to convey the spectrum to an external spectrometer. The standard spectrometer is an Insight spectrometer from Roper Scientific, 300 mm in focal length, with 300, 1200 and 2400 gr/mm gratings, and fitted with a Pixis cooled (-70°C) CDD, with a detector 1380x400 pixels, backthinned and UV coated.

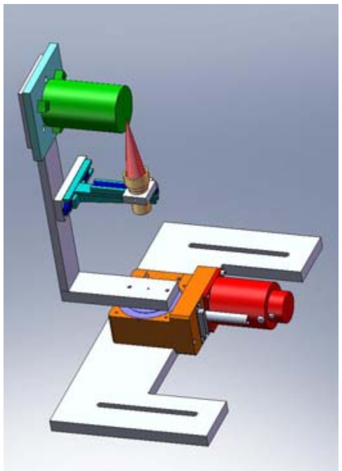

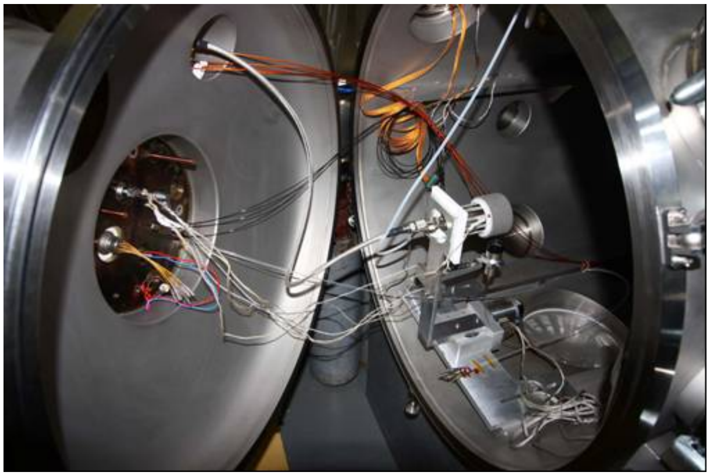

Figure 47. Beam scanning setup, including optics for emission spectra. CADview (top) and picture of the setup (bottom).

A picture of the thruster firing is shown in Figure 48.

Figure 48. Picture of the plume from the Helicon thruster (60Watt, 0.2 mg/s).

LIF setup

The setup, including an RPA, is shown in Figure 49. The thruster is mounted on three vacuum translation stages with 200mm range. Two detection optics and three laser optics are held by NewFocus vacuum actuated optical mounts. A CCD detector can be put in place of the thruster in vacuum to check the alignment of the laser beams and detection optics. An RPA is also available on a rotation stage.

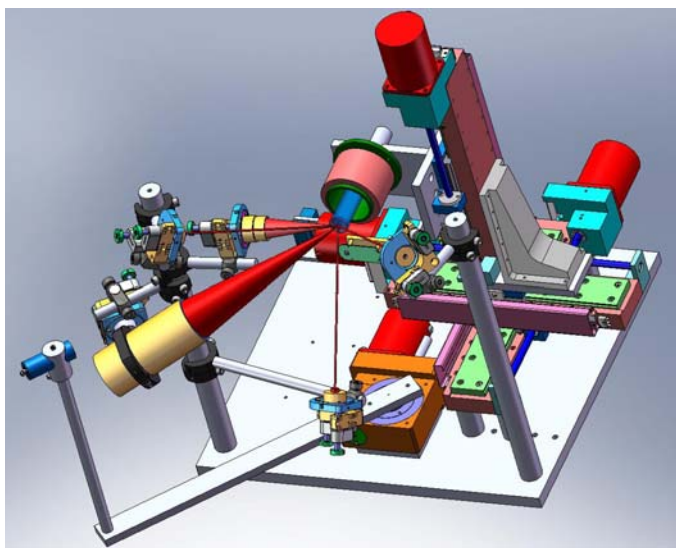

Figure 49. LIF setup. An RPA (blue) on a rotating arm is also included.

VIII. Conclusion

This paper has presented the experimental activities ongoing in the frame the of HPH.com research program to support the development for a mini helicon plasma thruster in the range 50-100 W. The experiments currently done have scanned a large number of parameters as source geometrical configuration, magnetic field topology and value, antenna type and feeding frequency. The large amount of data is now under evaluation to support the development of the qualification model. The results currently achieved allowed the development of an Engineering model which is currently under testing.

Weather the EM don't implement the most advanced solutions identified it is a very good test bed to support the technology development needed for the final qualification model ,

Acknowledgments

This research has been supported by the 7^{th} Framework Programme (FP7/2007-2013) of REA under grant agreement n° 218862 of the Helicon Plasma Hydrazine COmbined Micro (HPH.com) project.

References

1. O.V.Batishchev "Mini-Helicon Plasma Thruster Characterization" 44th AIAA/ASME/SAE/ASEE Joint Propulsion Conference & Exhibit 21 - 23 July 2008, Hartford, CT

2. C. Charles, R.W. Boswell, P. Alexander, C. Costa, O. Sutherland, L. Pfitzner, R. Franzen, J. Kingwell, A. Parfitt, P.E. Frigot, J. Gonzalez del Amo, E. Gengembre, G. Saccoccia, R. Walker "Helicon Double Layer Thrusters" 42nd. AIAA/ASME/SAE/ASEE Joint Propulsion Conference & Exhibit 9 - 12 July 200

3. D. Blackwell F. Chen "2D Imaging of a helicon discharge" Plasma Sources Sci. Technol. 6, 569 (1997).

4. D. Miljak F. Chen "Helicon wave excitation with rotating antenna fields" Plasma Sources Sci. Technol. 7, 61 (1998)

5. G.S. Eom, I.S. Hong, and Y.S. Hwang "DEVELOPMENT OF DC ACCELERATOR ION SOURCES USING HELICON PLASMAS" 1st Asian Particle Accelerator Conference (APAC 98), Tsukuba, Japan, 23-27 Mar 1998, pp 825.;

6. James H. Gilland, Gregory Piefer "Small Helicon Plasma Source Experiments" 40th AIAA/ASME/SAE/ASEE Joint Propulsion Conference and Exhibit 11 - 14 July 2004, Fort Lauderdale, Florida AIAA 2004-3939

7. O. V. Braginskii, A. N. Vasileva, and A. S. Kovalev Russian Microelectronics, Vol. 29, No. 6, 2000, pp. 380–390.

8. K. Toki1, T. Hashimoto K. Makita, S. Shinohara, T. Hada, Y. Ikeda, T. Tanikawa, K. Shamrai "Small Helicon Source for Electrodeless Plasma Production and Electromagnetic Acceleration "42nd AIAA/ASME/SAE/ASEE Joint Propulsion Conference & Exhibit 9 - 12 July 2006, Sacramento, California AIAA 2006-4843.

9. M. Yoshitaka "Study on Light-Ion Helicon Plasma Production with High-Density in Non-Uniform Magnetic Field " PhD thesys.

10. K. Shamrai*, Yury V. Virko†, Valery F. Virko‡, and Alexander I. Yakimenko Compact Helicon Plasma Source with Permanent Magnets for Electric Propulsion Application" 42nd AIAA/ASME/SAE/ASEE Joint Propulsion Conference & Exhibit 9 - 12 July 2006, Sacramento, California AIAA 2006-4845

11. T.Ziemba "High Power Heliocn Thruster " 41st AIAA/ASME/SAE/ASEE Joint Propulsion Conference and Exhibit 10-13 July 2005 Tucson Arizona AIAA 2005-4116

12. O. Batishchev "Minihelicon Plasma Thruster"IEEE Transactions on plasma science, VOL. 37, NO. 8, AUGUST 2009 1563

13. F. Chen and H. Torreblanca "Large-area helicon plasma source with permanent magnets" Plasma Phys. Control. Fusion 49 (2007) A81–A93 doi:10.1088/0741-3335/49/5A/S07

14. M. Light F. Chen P. L. Colestock "Low frequency electrostatic instability in a helicon plasma" Physics Of Plasmas volume 8, number 10 october 2001

15. J. Kline "Resonant Ion Heating in a Helicon Plasma" MSC THESIS

16. S. Shinohara, T. Tanikawa "Development of Very Large Helicon Plasma Source" Review of Scientific Instruments volume 75, number 6 june 2004

17. J. M. Pucci, N. Sinenian, J. Palaia, M. Celik, Z. LaBry A. Shabshelowitz O. Batishchev and M. Martinez-Sanchez "Preliminary Characterization of a Helicon Plasma Source for Space Propulsion" 42nd AIAA/ASME/SAE/ASEE Joint Propulsion Conference & Exhibit 9 - 12 July 2006, Sacramento, California AIAA 2006-5255.

18. K. Toki, S. Shinohara, T. Tanikawa, K. Shamrai "Small helicon plasma source for electric propulsion" Thin Solid Films 506– 507 (2006) 598 597–600.

19. S. Shinohara H.Mizokoshi "Development of a strong field helicon plasma source " Review of Scientific Instruments 77, 036108 _2006.

20. S. Pottinger, T. Harle, V. Lappas, W. Cox, T. Lafleur, P. Alexander, C. Charles, R. Boswell, M. Perren, R. Laine *Helicon double layer thruster development for low power operation*, Space Propulsion Conference 3-6 May 2011 San Sebastian Spain.

[21] K. Katsonis, Ch. Berenguer, D. Pavarin, A. Lucca Fabris, F. Trezzolani, M. Faenza, P. Tsekeris, S. Cohen, M. Cornille, *Optical Diagnostics of a Low Temperature Argon Thruster*, IEPC11 Conference, September 11 – 15, 2011, Wiesbaden (Germany) IEPC-2011-169
[22] Pavarin, F. Ferri, M. Manente, D. Curreli, Y. Güçlü, D. Melazzi, D. Rondini, S. Suman, J. Carlsson, C. Bramanti, E. Ahedo, V. Lancellotti, K. Katsonis, G. Markelov, *Design of 50 W Helicon Plasma Thruste*r, IEPC-2009-205, 31th IEPC Conference, Sept. 2009, Ann Arbor, MI, USA
[23] K. Katsonis, Ch. Berenguer, M. Cornille, *Atomic Data in Ar Thruster Multidimensional Modeling and Optical Diagnostics*, IEPC-2009-035, 31th IEPC Conference, Sept. 2009, Ann Arbor, MI, USA
[24] O. Tudisco, A. Lucca Fabris, C. Falcetta, L. Accatino, C. Neri, F. Pollastrone, M. Florean, R. De Angelis, C. Mazzotta, A.A. Tuccillo, M.Faenza, F. Ferri, D. Pavarin, A. Selmo, L. Tasinato and F.Trezzolani, *Very highly sensitive microwave interferometer for tenuous plasma density measurements*., to be submitted.
[25] Kristina M. Lemmer, Alec D. Gallimore, Timothy B. Smith and Daniel R. Austin, *Review of Two Retarding Potential Analyzers for Use in High Density Helicon Plasma*, 30th International Electric Propulsion Conference 17-20 September 2007 Florence Italy.
[26] Christian Böhm and Jérôme Perrin. Retarding-field analyzer for measurements of ion energy distributions and secondary electron emission coefficients in low-pressure radio frequency discharges. *Review of Scientific Instruments*, 64(1):31–44, 1993.